THE JOURNAL OF PHYSICAL CHEMISTRY B

Article

pubs.acs.org/JPCB

Reactions of Th^+ + H_2, D_2, and HD Studied by Guided Ion Beam Tandem Mass Spectrometry and Quantum Chemical Calculations

Richard M Cox,[†] P. B. Armentrout,[*,†] and Wibe A. de Jong[‡]

[†]Department of Chemistry, University of Utah, Salt Lake City, Utah 84112-0850 United States

[‡]Lawrence Berkeley National Laboratory, One Cyclotron Road, Berkeley, California 94720, United States

S Supporting Information

ABSTRACT: Kinetic energy dependent reactions of Th^+ with H_2, D_2, and HD were studied using a guided ion beam tandem mass spectrometer. Formation of ThH^+ and ThD^+ is endothermic in all cases with similar thresholds. Branching ratio results for the reaction with HD indicate that Th^+ reacts via a statistical mechanism, similar to Hf^+. The kinetic energy dependent cross sections for formation of ThH^+ and ThD^+ were evaluated to determine a 0 K bond dissociation energy (BDE) of $D_0(Th^+-H) = 2.45 \pm 0.07$ eV. This value is in good agreement with a previous result obtained from analysis of the Th^+ + CH_4 reaction. $D_0(Th^+-H)$ is observed to be larger than its transition metal congeners, TiH^+, ZrH^+, and HfH^+, believed to be a result of lanthanide contraction. The reactions with H_2 were also explored using quantum chemical calculations that include a semiempirical estimation and explicit calculation of spin−orbit contributions. These calculations agree nicely and indicate that ThH^+ most likely has a $^3\Delta_1$ ground level with a low-lying $^1\Sigma^+$ excited state. Theory also provides the reaction potential energy surfaces and BDEs that are in reasonable agreement with experiment.

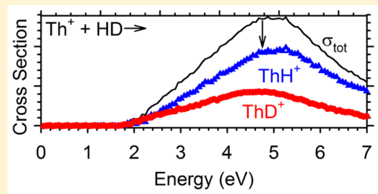

■ INTRODUCTION

There is considerable interest in actinide chemistry, although the radioactivity of most actinides (except Th and U) has limited their study to dedicated laboratories. As a consequence, actinide chemistry in the gas phase, in particular, where fundamental actinide chemistry can be studied absent solvent effects, is still largely in its infancy. To date, most experimental work has dealt with oxidation[1−9] and hydrocarbon activation reactions.[10−18] The dearth of experimental work has led to increased theoretical studies of actinides in the gas phase.[17,19−29] Although the use of theoretical methods to study actinide systems mitigates safety concerns, the limited experimental data leaves few benchmarks to which theoretical methods can be compared. Several examples of discrepancies (real or apparent) between experimental results and theoretical methods can be found in the literature.[24−26,30] Some of these discrepancies can be traced to errors in the experimental work;[26] others appear to be method or basis set related.[24,25,30]

In order to provide experimental benchmarks for comparison to theoretical work, Heaven and collaborators have recently studied several simple Th and U molecules spectroscopically, as summarized in ref 31. In our group, we have used guided ion beam tandem mass spectrometry to study the reaction of Th^+ + CH_4, which leads to thermodynamic bond dissociation energies (BDEs) for several species.[30] A simple actinide system that can be studied in detail both experimentally and theoretically is the reaction with H_2 and its isotopic analogues. This system is of interest, in part, because it provides the simplest example of covalent bond activation by metal cations, and deuterium labeling provides experimental insight into the reaction mechanism. Periodic trends in this chemistry are also of interest as the M^+ + H_2 reaction has been extensively studied for first-row,[32−39] second-row,[36,39−41] and third-row[42−46] transition metals.

Because all the lanthanides (Ln) can be studied without radioactivity concerns (with the exception of Pr where all known isotopes are radioactive), they can be considered model systems to shed light on the analogous actinide systems. Of the lanthanides and actinides, only the reactions of La^+, Yb^+, Lu^+ + H_2, and U^+ + D_2 have been studied experimentally.[10,39,47,48] LnH^+ formation has also been observed in reactions of many Ln^{2+} with alkanes and alkenes, as studied using ion cyclotron resonance (ICR) mass spectrometry.[49] Additionally, LaH^+ and LuH^+ have been observed as products in reactions of La^+ and Lu^+ with methane and ethane in guided ion beam experiments.[39,48] For the actinides, AnH^+ (An = U, Np, Pu, Am, Cm) has been observed as a product of An^{2+} reacting with alkanes and alkenes in ICR experiments, but ThH^+ was not observed in analogous experiments.[17,18] Recently, we have observed ThH^+ in a guided ion beam study of the Th^+ + CH_4 reaction.[30] Here we report the absolute cross sections as a function of kinetic energy for the reactions of H_2, D_2, and HD with Th^+. Analysis of these cross sections allows determination of $D_0(Th^+-H)$. Theoretical calculations of ThH^+ and ThH_2^+ are also performed to assign electronic states and explore possible reaction mechanisms.

Special Issue: Bruce C. Garrett Festschrift

Received: August 17, 2015
Revised: September 25, 2015
Published: September 28, 2015

DOI: 10.1021/acs.jpcb.5b08008
J. Phys. Chem. B 2016, 120, 1601−1614

EXPERIMENTAL AND THEORETICAL METHODS

Instrument. The guided ion beam tandem mass spectrometer used in this study has been described in detail previously.[50] Briefly, thorium ions are created using a direct current discharge/flow tube source (DC/FT)[51] described in further detail below. Ions are extracted and focused through a magnetic momentum analyzer where the $^{232}Th^+$ beam is mass selected before being decelerated to a well-defined kinetic energy. The Th^+ beam is then focused into a radio frequency (rf) octopole guide that traps ions radially.[52,53] This octopole passes through a static pressure gas cell that contains the neutral gas reactant. To ensure that the probability of multiple collisions is sufficiently small, pressures are kept low (0.05–0.40 mTorr). Reactions were repeated at several pressures to ensure that the reported cross sections are independent of neutral gas pressure. After the collision cell, product ions and remaining reactant ions drift to the end of the octopole where they are extracted, focused through a quadrupole mass filter for mass analysis, and counted using a Daly detector.[54] Reaction cross sections are calculated from product ion intensities relative to reactant ion intensities after correcting for background ion intensities after the neutral gas is no longer directed into the gas cell.[55] Uncertainties in the calculated absolute cross section are estimated to be ±20%, with relative uncertainties of ±5%.

Laboratory ion energies (lab) are converted to the center-of-mass frame (CM) using the relationship $E_{CM} = E_{lab} \times m/(m + M)$ where m and M are the masses of the neutral and ionic reactants, respectively. Cross sections are known to be broadened by the kinetic energy distribution of the reactant ions and the thermal (300 K) motion of the neutral reactant.[56] The absolute zero of energy and the full width at half-maximum (fwhm) of the ion beam are determined by using the octopole guide as a retarding potential analyzer.[55] Typical fwhms of the energy distribution for these experiments were 0.4–0.8 eV (lab). Uncertainties in the absolute energy scale are 0.1 eV (lab). All energies reported below are in the CM frame.

Ion Source. The DC/FT source is described in detail elsewhere.[51] A cathode, held at 2.5 kV and containing a thorium powder sample, creates an electric field that ionizes Ar from the carrier gas. Ar cations collide with the thorium sample such that Th^+ sputters off the cathode. Ions are swept into a 1 m long flow tube by a 9:1 mixture of He/Ar at a total pressure of 0.2–0.5 Torr. The ions undergo ∼10^5 collisions with the flow gases, which should thermalize them. No evidence of excited states is evident in the reaction cross sections presented below nor in our previous work on $Th^+ + CH_4$.[30] Previous experiments have indicated that atomic ions generated in the DC/FT may have internal electronic temperatures between 300 and 1100 K.[41,57–60] A population analysis at 300 K indicates that 99.89% of Th^+ is in its ground level ($^4F_{3/2}$, $6d^27s$), whereas at 1100 K, 76% is in the ground level.[30] Conservatively, we estimate the internal temperature distribution of Th^+ as 700 ± 400 K, such that the internal energy of the reactant ions is 0.02 ± 0.03 eV.

Data Analysis. The kinetic energy dependence of endothermic reactions is modeled using eq 1[61–63]

$$\sigma(E) = \sigma_0 \sum g_i (E + E_i - E_0)^n / E \quad (1)$$

where σ_0 is an energy independent scaling factor, E is the relative kinetic energy of the reactants, E_i is the internal energy of the reactant states (electronic for Th^+ and rotational for H_2, D_2, and HD) having populations g_i ($\sum g_i = 1$), n is an adjustable parameter, and E_0 is the 0 K reaction threshold. Before comparison to the data, eq 1 is convoluted over the kinetic energy distributions of the reactants, and the σ_0, n, and E_0 parameters are optimized using a nonlinear least-squares method to best reproduce the experimental cross section. Uncertainties in E_0 are calculated from the threshold values from several independent data sets (minimum of two for each system) and combined with the absolute uncertainties in the kinetic energy scale (<0.002 eV) and internal energies of reactant ions (0.02 ± 0.03 eV). Thresholds are used to determine the bond dissociation energy (BDE), $D_0(Th^+–H)$, using eq 2 and its isotopic analogues.

$$D_0(Th^+{-}H) = D_0(H{-}H) - E_0 \quad (2)$$

Equation 2 assumes that there are no barriers in excess of the endothermicity of the reaction. No experimental or theoretical evidence was found to suggest that such a barrier is present.

Theoretical Approaches. Most quantum chemical calculations are performed using the Gaussian 09 suite of programs.[64] Unless otherwise noted, a correlation consistent polarized core (20s17p12d11f7g4h1i)/[9s9p8d8f7g4h1i] basis set (cc-pwCVQZ-MDF) developed by K.A. Peterson[65] that utilizes the Stuttgart–Cologne (MDF) fully relativistic small core (60 electron) ECP[66] is used for Th along with the aug-cc-pVQZ[67] basis set for H. For calculating bond dissociation energies, several additional basis sets are used for Th^+ and H. For Th^+, these include the Stuttgart Dresden basis set (SDD-VDZ-MWB) with its accompanying small core quasirelativistic ECP (MWB) available on the EMSL basis set exchange,[68,69] a segmented basis set (Seg. SDD-VQZ-MWB) that utilizes the MWB ECP,[70] atomic natural orbital basis sets designed for use with the MWB (ANO-VQZ-MWB)[70] and MDF (ANO-VQZ-MDF)[66] ECPs, and correlation consistent cc-pVTZ-MDF, cc-pVQZ-MDF, and cc-pwCVTZ-MDF (which includes core–valence correlation) basis sets[65] with the MDF ECP. Pople 6-311+G(3p), cc-pVTZ, and cc-pVQZ basis sets[67] are also used for H. Additionally, BDEs are calculated using single point energies utilizing the all-electron variants of cc-pVXZ (cc-pVXZ-DK3) and cc-pwCVXZ (cc-pwCVXZ-DK3) basis sets[65] (where X = T or Q) and B3LYP/cc-pwCVQZ-MDF/aug-cc-pVQZ optimized structures. These latter calculations are performed using the second order Douglas–Kroll–Hess Hamiltonian (DK2).[71–76] Of note is that the all-electron basis sets were formulated for use with a third order Douglas–Kroll–Hess Hamiltonian (DK3), but the DK3 calculations cannot be performed presently in the current setup. Use of the DK2 may lead to errors, but we anticipate that these errors should be small.[77] Extrapolation to the complete basis set limit (CBS) is performed using the Karton–Martin method,[65,78] eq 3, proposed for the HF energies with the TZ ($X = 3$) and QZ ($X = 4$) energies:

$$E_X = E_{CBS} + A(X + 1)e^{-6.57\sqrt{X}} \quad (3)$$

For CCSD(T) calculations, eq 4[65,79,80] is used to extrapolate the correlation energy:

$$E_X = E_{CBS} + B\left(X + \frac{1}{2}\right)^{-4} \quad (4)$$

The calculations utilize the density functional theory (DFT) methods B3LYP, B3PW91, BHandHLYP (BHLYP), M06, and PBE0. Of these functionals, B3LYP has been shown to perform well in similar systems.[28,30] B3PW91 has been shown by us[30] and others[24] to perform reasonably well in other actinide systems. BHLYP has been shown to perform well in singly bound metal ligand systems.[44,45,81] M06 recently performed well in a theoretical evaluation of several DFT methods by comparison to the experimental $D_0(OTh^+{-}O)$.[28] PBE0 has previously yielded similar geometrical structures to B3LYP in our previous Th^+ study.[30] Additionally, a coupled cluster method that mixes single and double excitations with perturbative triple excitations (CCSD(T)) was used for single point calculations using the B3LYP optimized structures. For CCSD(T) electron correlation calculations, the 5s and 5p electrons are frozen. All calculations are open-shell and unrestricted, and all energies discussed below are corrected by the zero point energy using the frequencies generated for their respective optimized structure after scaling by 0.989.[82] Representative energies (and zero point energies) from B3LYP/cc-pwCVQZ-MDF/aug-cc-pVQZ calculations are listed in Table S1 in the Supporting Information. No significant spin contamination was observed in these calculations for any species studied except for Th^+ (^2D, $6d7s^2$) for all calculations (and basis sets) except M06 and for Th^+ (^2F, $5f7s^2$) calculated at the B3LYP/cc-pwCVQZ-DK3 level (see Table S2 in the Supporting Information for representative $s(s + 1)$ values).

■ EXPERIMENTAL RESULTS

Th^+ + H_2 and D_2. The reactions of Th^+ with H_2 and D_2 yield products according to reactions 5 and 6.

$$Th^+ + H_2 \rightarrow ThH^+ + H \tag{5}$$

$$Th^+ + D_2 \rightarrow ThD^+ + D \tag{6}$$

The kinetic energy dependent cross section for reaction 5 can be found in Figure 1 with the analogous deuterium cross section in Figure 2. Reactions 5 and 6 have apparent thresholds near 2 eV with the cross sections peaking near $D_0(H{-}H)$ = 4.478 eV and $D_0(D{-}D)$ = 4.556 eV.[83] Above these energies, the cross sections decrease because the ThH^+ and ThD^+ products can dissociate leading to Th^+ + 2H (2D).

The mass resolution settings in the quadrupole for both the H_2 and D_2 (as well as HD) reactions were constant. Resolution was held as low as possible to ensure efficient product collection, such that the product ion peaks overlap with the reactant ion peak, with the overlap being worse for ThH^+ than ThD^+, which explains why the H_2 data is somewhat noisier. In the present case, the magnitude at the maximum ThH^+ cross section, Figure 1, is 1.2 times that for ThD^+, Figure 2. This is within the estimated absolute cross section uncertainty (±20%) indicating that the resolution settings are adequate for accurately measuring the product ion intensities.

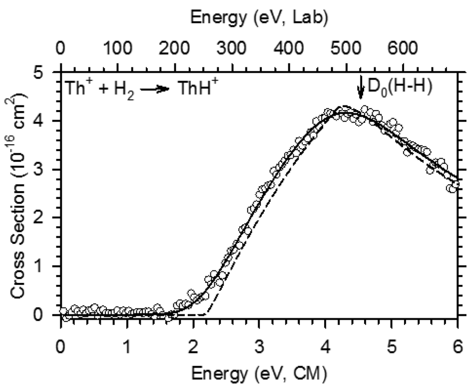

Figure 1. Cross sections for the reaction between Th^+ and H_2 as a function of energy in the center-of-mass (lower x-axis) and laboratory (upper x-axis) frames. The model of eq 1 with parameters from Table 1 is shown as a dashed line. This model convoluted over the kinetic energy and internal energy distributions of the reactants is shown as a solid line. The arrow indicates $D_0(H{-}H)$ = 4.478 eV.

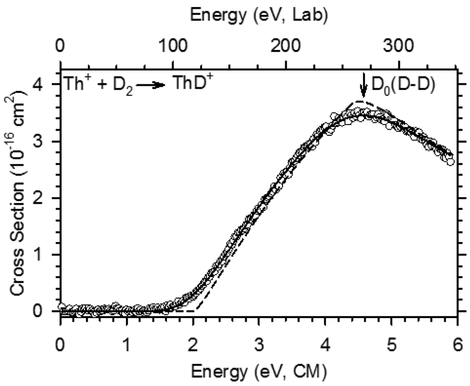

Figure 2. Cross sections for the reaction between Th^+ and D_2 as a function of energy in the center-of-mass (lower x-axis) and laboratory (upper x-axis) frames. The model of eq 1 with parameters from Table 1 is shown as a dashed line. This model convoluted over the kinetic energy and internal energy distributions of the reactants is shown as a solid line. The arrow indicates $D_0(D{-}D)$ = 4.556 eV.

Th^+ + HD. Reaction of Th^+ with HD yields products according to reactions 7 and 8.

$$Th^+ + HD \rightarrow ThH^+ + D \tag{7}$$

$$\rightarrow ThD^+ + H \tag{8}$$

The cross sections measured for these reactions are shown in Figure 3. Reactions 7 and 8 have similar apparent thresholds as reactions 5 and 6 and peak near $D_0(H{-}D)$ = 4.514 eV.[83] At energies somewhat above the apparent thresholds, ThH^+ is found to be the dominant product by a 2:1 ratio. The magnitude of the total cross section, Figure 3, is 0.8 times the magnitude of the cross section for reaction 6, Figure 2, also within experimental uncertainty.

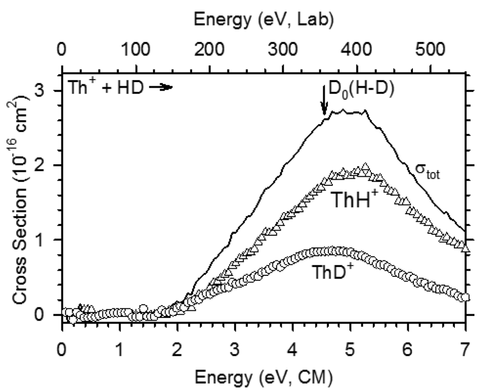

Figure 3. Cross sections for the reaction between Th^+ and HD as a function of energy in the center-of-mass (lower x-axis) and laboratory (upper x-axis) frames. The arrow indicates $D_0(H{-}D)$ = 4.514 eV.

Thermochemical Results. The fitting parameters from eq 1 used to model the cross sections in reactions 5−8 can be

DOI: 10.1021/acs.jpcb.5b08008
J. Phys. Chem. B 2016, 120, 1601−1614

found in Table 1. The models for reactions 5 and 6 are included in Figures 1 and 2 and can be seen to reproduce the data throughout the energy range examined. Above the neutral reactant bond energy, product ions can have enough internal energy to dissociate. To account for this effect, eq 1 is augmented with a simple model for dissociation, detailed elsewhere.[63,84] Because the model of eq 1 explicitly accounts for the internal energy of all reactants, the E_0 values reported in Table 1 are 0 K thresholds. It can be seen that the thresholds for all four reactions are similar. Given D_0(H−H) = 4.478 ± 0.001 eV and D_0(D−D) = 4.556 ± 0.001 eV[83] in eq 2, the thresholds measured for reactions 5 and 6 indicate that $D_0(Th^+{-}H)$ = 2.30 ± 0.12 eV and $D_0(Th^+{-}D)$ = 2.54 ± 0.05 eV. Using eq 2 and D_0(H−D) = 4.514 ± 0.001 eV[83] leads to $D_0(Th^+{-}H)$ = 2.36 ± 0.06 eV and $D_0(Th^+{-}D)$ = 2.38 ± 0.19 eV. After correcting for zero point energy differences of 0.03 eV, the weighted average of these four measurements is $D_0(Th^+{-}H)$ = 2.45 ± 0.07 eV, where the uncertainty is two standard deviations of the mean.

Table 1. Fitting Parameters of Equation 1 for the Indicated Reaction Cross Section

reaction	n	σ_0	E_0 (eV)	$D_0(Th^+{-}H)$[a]
$Th^+ + H_2 \rightarrow ThH^+ + H$	1.3 ± 0.3	7.6 ± 1.3	2.18 ± 0.12	2.30 ± 0.12
$Th^+ + D_2 \rightarrow ThD^+ + D$	1.4 ± 0.1	4.6 ± 0.6	2.02 ± 0.05	2.51 ± 0.05
$Th^+ + HD \rightarrow ThH^+ + D$	1.4 ± 0.1	2.2 ± 0.2	2.15 ± 0.06	2.36 ± 0.06
$Th^+ + HD \rightarrow ThD^+ + H$	1.2 ± 0.1	1.3 ± 0.2	2.13 ± 0.19	2.35 ± 0.19

[a]Values derived from reactions forming ThD^+ include a zero point energy correction of −0.03 eV. All values in eV.

This result is in good agreement with the value, $D_0(Th^+{-}H)$ ≥ 2.25 ± 0.20 eV, measured in the reaction of Th^+ with CH_4.[30] The present value is considered more reliable because there are no competing products, unlike in the methane reaction where the $ThH^+ + CH_3$ channel competes with the thermodynamically more favored dehydrogenation channel, $ThCH_2^+ + H_2$. In that study, a phase space theory (PST) model of the cross sections of products that share a common intermediate ($ThCH_2^+$, $ThCH_3^+$, and ThH^+) was used to account for this competition. This model explicitly accounts for angular momentum conservation and statistical factors by utilizing the theoretically calculated molecular parameters (vibrational and rotational) of all products and reactants. The PST analysis yielded a threshold energy for ThH^+ formation of E_0 = 2.05 eV indicating $D_0(Th^+{-}H)$ = 2.45 eV,[30] in excellent agreement with the present value.

Reaction Mechanism. Previous work with transition metals has shown that the M^+ + HD branching ratio is very sensitive to the reaction mechanism.[40,41,85] Three guidelines have been established to predict the following reaction mechanism: (1) If M^+ has an electronic configuration with empty s and dσ orbitals, such as a d^n configuration where $n < 5$, the reaction proceeds efficiently by an insertion mechanism. These processes are consistent with the statistical behavior of a long-lived covalently bound HMH^+ intermediate that allows energy to be redistributed throughout the intermediate statistically and have branching ratios ($\sigma_{MH^+}/\sigma_{Tot}$) near 0.5. (2) If M^+ has an electronic configuration with occupied valence s or dσ orbitals and is low-spin, such as for d^n where $n > 5$ or low-spin coupled $d^{n-1}s^1$ configurations, the reaction proceeds efficiently via a direct mechanism. These processes are consistent with a short-lived interaction between $M^+ + H_2$ such that conservation of angular momentum favors MH^+ by factors of 2−4 such that $\sigma_{MH^+}/\sigma_{Tot}$ is typically between 0.66 and 0.80.[32,48,86,87] (3) If M^+ has an electronic configuration with occupied valence s or dσ orbitals and has the highest possible spin state, such as a high-spin coupled $d^{n-1}s^1$ configuration, the reaction proceeds inefficiently by an impulsive mechanism in which M^+ interacts strongly with either H or D but not both. Such processes favor MD^+ + H by a large factor. However, these rules are only appropriate for strictly diabatic behavior where the M^+ electronic configuration is essentially static through the course of the reaction.

Figure 4 compares the branching ratio, $\sigma_{MH^+}/\sigma_{Tot}$, for Th^+ with the group 4 transition metal cations. Given that both Ti^+ and Zr^+ have ^4F (d^2s) ground states, an impulsive mechanism according to category 3 is expected. However, Figure 4 clearly indicates a statistical (category 1) reaction for Ti^+. This can be explained by coupling with the low-lying ^4F ($4d^3$) state, which is then expected to react according to the first guideline. Zr^+ has a reactivity consistent with a direct mechanism (category 2). This is explained by the coupling of the high-spin surfaces evolving from ground state Zr^+ (^4F, $4d^25s$) + H_2 with the low-spin surfaces that lead to the intermediates and products.[41] For Hf^+, the ground state is ^2D ($5d6s^2$) indicating that an impulsive mechanism is expected. However, the $HHfH^+$ PES indicates that coupling occurs between low-spin surfaces originating from the ground state reactants and a $^2A_1$ surface that leads to a long-lived $HHfH^+$ intermediate, which can evolve directly to products.[44] This is substantiated by the results in Figure 4.

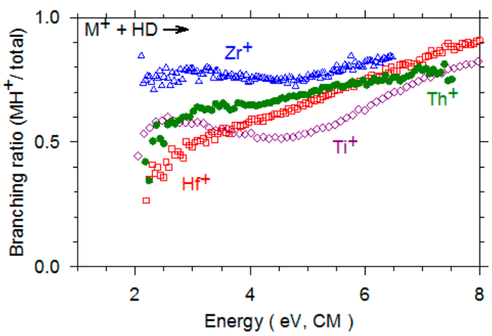

Figure 4. Product branching fractions ($\sigma_{MH+}/\sigma_{Total}$) for reactions of Ti^+ (purple ◇), Zr^+ (blue △), Hf^+ (red □), and Th^+ (green ●) with HD as a function of kinetic energy in the CM frame.

Interestingly, for Th^+, the $\sigma_{MH^+}/\sigma_{Tot}$ ratio is between that of Hf^+ and Zr^+, Figure 4. The Th^+ ground state is enigmatic because the ground level is a mixture of the $^4F_{3/2}$ ($6d^27s$) and $^2D_{3/2}$ ($6d7s^2$).[88] Like Zr^+ and Hf^+, it appears that the $Th^+ + H_2$ ground state reactants evolve along surfaces starting from the mixed character of the $J = {}^3/_2$ ground level and coupling with low-spin surfaces leading to a long-lived $HThH^+$ intermediate (category 1).

For all metals, the branching ratio increasingly favors MH^+ + D formation at energies above D_0(H−D) = 4.51 eV. This trend has been explained previously,[32] and is a consequence of the heavier D atom's ability to carry away more energy than the lighter H atom.

DOI: 10.1021/acs.jpcb.5b08008
J. Phys. Chem. B 2016, 120, 1601−1614

Table 2. Comparison of Theoretically Computed Excited State Energies (eV) to Experimental Values for Th^+[a]

Th^+	exptl[b]	CCSD(T)	B3LYP	B3PW91	BHLYP	M06	PBE0
^2D ($6d7s^2$)[c]	**0.00**	**0.00 (0.00)**	0.06 (0.12)	**0.00 (0.00)**	**0.00 (0.00)**	0.73	**0.00 (0.00)**
^4F ($6d^27s$)	0.06	0.16 (0.13)	0.26 (0.13)	0.04 (0.08)	0.19 (0.19)	1.39	0.04 (0.02)
^2F ($5f7s^2$)	0.43	0.57	**0.00 (0.00[d])**	0.15	0.32	**0.00**	0.20
^4H (5f6d7s)	0.67	1.17	0.45	0.29	0.74	1.24	0.36
^4F ($6d^3$)	0.81	0.98	1.04	0.73	0.93	1.81	0.72

[a]Calculated using cc-pwCVQZ-MDF basis set. Values in parentheses calculated using the cc-pwCVQZ-DK3 all-electron basis set. Bold values highlight the ground state. [b]Experimental energies are averaged over all spin−orbit levels and are taken from refs 88 and 89. Also see Supporting Information of ref 30. [c]Significant spin contamination, s(s+1) ~ 1.5, except for M06 (see Table S2). [d]Significant spin contamination, s(s+1) ~ 1.1.

Table 3. Molecular Parameters and Calculated Relative Energies (eV) for Ground and Excited States of ThH^+[a]

ThH^+	$r(Th^+–H)$ (Å)[b]	ν (cm^{-1})[b]	CCSD(T)[c]	B3LYP	B3PW91	BHLYP	M06	PBE0
$^3\Delta_1$ ($\sigma^2\sigma\delta$)[d]	1.996	1653	**0.00** (0.05)	**0.00 (0.00)**	**0.00 (0.00)**	**0.00 (0.00)**	0.10 (0.28)	**0.00 (0.00)**
$^1\Sigma^+$ ($\sigma^2\sigma^2$)	1.946	1592	0.13 **(0.00)**	0.45 (0.27)	0.69 (0.51)	0.46 (0.28)	**0.00 (0.00)**	0.68 (0.50)
$^3\Pi_0$ ($\sigma^2\sigma\pi$)[e]	2.001	1604	0.38 (0.35)	0.29 (0.20)	0.32 (0.23)	0.35 (0.26)	0.27 (0.36)	0.33 (0.24)
$^3\Phi_2$ ($\sigma^2\delta\pi$)[f]	2.032	1491	0.61 (0.75)	0.63 (0.72)	0.57 (0.66)	0.61 (0.70)	0.44 (0.71)	0.57 (0.66)
$^3\Sigma^-$ ($\sigma^2\delta^2$)	2.029	1547	0.96 (0.83)	1.03 (0.85)	0.98 (0.80)	1.04 (0.86)	0.97 (0.97)	0.97 (0.79)
$^3\Sigma^-$ ($\sigma^2\pi^2$)	2.014	1509	1.11(0.98)	1.21 (1.03)	1.10 (0.92)	1.17 (0.99)	0.98 (0.98)	1.09 (0.91)

[a]Structures optimized using cc-pwCVQZ-MDF/aug-cc-pVQZ at the respective level of theory (except CCSD(T)) relative to the ground level (state) with the ground level (state) bolded. Values include spin−orbit correction to the lowest level of each state where applicable. Values in parentheses do not include spin−orbit corrections. [b]From B3LYP/cc-pwCVQZ-MDF/aug-cc-pVQZ optimized structures. Frequencies scaled by 0.989. [c]Single point energy from B3LYP/cc-pwCVQZ-MDF/aug-cc-pVQZ optimized structures. [d]Includes spin−orbit correction of −0.18 eV. [e]Includes spin−orbit correction of −0.09 eV. [f]Includes spin−orbit correction of −0.27 eV.

THEORETICAL RESULTS

Energy Levels of Th^+. One way to gauge the accuracy of a theoretical method is to compare predicted low-lying states to those observed experimentally. Previously, this has been done for the atomic Th^+ cation[20,21,24,30] using several basis sets at various levels of theory. A comparison of the theoretically predicted low-lying states calculated using the cc-pwCVQZ-MDF basis set to those experimentally observed is listed in Table 2. For comparison to the theoretical values, the experimental levels were averaged over all spin−orbit levels of each state.[88,89] For Th^+, this is not straightforward because of considerable interaction between the ^4F ($6d^27s$) and ^2D ($6d7s^2$) states. A detailed explanation of the choice of each level has been given previously in the Supporting Information section of ref 30.

With the exception of M06 and B3LYP, which prefer the ^2F state, all levels of theory correctly predict a ^2D ground state. Furthermore, BHLYP, B3PW91, and PBE0 correctly predict the ordering of all states. However, for these approaches, the spacing between states is smaller than that observed experimentally (particularly so for B3PW91). Although CCSD(T) incorrectly places the ^4H (5f6d7s) higher in energy than the ^4F ($6d^3$), it otherwise correctly orders the states. CCSD(T) reproduces the correct spacing between the states, deviating from the excited experimental states by only 0.10−0.17 eV when excluding the ^4H. Additionally, the relative energies of the ^2D and ^4F states were calculated using the all-electron cc-pwCVQZ-DK3 basis set for Th^+ and are also listed in Table 2. (M06 calculations did not converge and are not included here.) These results are similar to cc-pwCVQZ-MDF values.

Spin−Orbit Energy Corrections. Typically, theoretical BDEs correspond to a value that has been averaged over all spin−orbit states whereas experimental 0 K BDEs correspond to dissociation from the lowest levels of the molecule to its fragments. In order to make a more valid comparison between experimental and theoretical values, spin−orbit effects, which are quite large for Th^+, must be explicitly accounted for. Here we employ a semiempirical approach to estimate the spin−orbit effects in the ThH^+ system. This approach has been used successfully to estimate spin−orbit effects in third-row transition metal systems and another Th^+ system.[30,90−93] These corrections require that the Th^+ + H asymptote be lowered by the empirical difference between the ground level of Th^+ and the ground state energy averaged over all spin−orbit levels. A nuance of the Th^+ system is that the experimental ground state is ^2D ($6d7s^2$) whereas the ground level is $^4F_{3/2}$ ($6d^27s$).[30] This allows two possible approaches for correcting BDEs. The first is to assume that the theoretical BDE is robust along the diabatic dissociation surface. This necessitates that the BDE must be referenced to its diabatic asymptote and corrected by the empirical difference in energy between the $^4F_{3/2}$ ground level and the average energy of the respective state, 0.46 eV for ^4F and 0.40 eV for ^2D. The second approach corrects directly from the ^2D ground state to the $^4F_{3/2}$ ground level by the empirical difference (0.40 eV). Previously, the latter method yielded slightly better results and as such is the method used here.[30]

In addition to the spin−orbit correction to the asymptote, the BDE should also be corrected for the spin−orbit splitting of ThH^+ when applicable.[30,90−93] To do so, we assume that the spin−orbit splitting energy is given by eq 9:

$$E^{SO} = \Lambda M_S A \quad (9)$$

Here A is the spin−orbit splitting constant, Λ is the orbital angular momentum quantum number, and M_S is the spin quantum number associated with a particular level $\Omega = \Lambda + M_S$.[94] E^{SO} is also equal to the summation $\sum a_i l_i \cdot s_i$, where $l_i \cdot s_i$ is the dot product of the orbital angular momentum and the spin of electron i and a_i is the spin−orbit parameter, which can be represented by the atomic spin−orbit parameter for the 6d

Table 4. Theoretical BDEs (eV) of ThH^+[a]

basis set	CCSD(T)[b,c]	B3LYP[c]	B3PW91[c]	BHLYP[c]	M06[d]	PBE0[c]
SDD-VDZ-MWB/6-311+G(3p)	2.42	2.88	2.91	2.73	2.69	2.83
Seg. SDD-VQZ-MWB/6-311+G(3p)	2.57	2.94	2.96	2.77	2.74	2.89
ANO-VQZ-MWB/6-311+G(3p)	2.57	2.92	2.95	2.75	2.72	2.87
ANO-VQZ-MDF/6-311+G(3p)	3.43	2.92	2.94	2.77	2.73	2.87
cc-pwCVQZ-MDF/aug-cc-pVQZ	2.71	2.89	2.91	2.75	2.73	2.84
cc-pwCVTZ-MDF/cc-pVTZ	2.64	2.89	2.91	2.75	2.71	2.85
cc-pwCVQZ-MDF/cc-pVQZ	2.69	2.89	2.91	2.75	2.72	2.84
CBS-cc-pwCVXZ-MDF[e]	2.72	2.89	2.91	2.75	2.72	2.84
cc-pVTZ-DK3/cc-pVTZ[f]	2.74	2.78	2.87	2.75		2.85
cc-pVQZ-DK3/cc-pVQZ[f]	2.80	2.79	2.87	2.75		2.86
CBS-cc-pVXZ-DK3[e]	2.83	2.79	2.87	2.75		2.85
cc-pwCVTZ-DK3/cc-pVTZ[f]	2.64	2.90	2.87	2.75		2.85
cc-pwCVQZ-DK3/cc-pVQZ[f]	2.69	2.90	2.87	2.75		2.85
CBS-cc-pwCVXZ-DK3[e]	2.72	2.90	2.88	2.75		2.85

[a]Calculated from structures optimized using the indicated basis sets (Th^+ basis set, ECP/H basis set) at the respective level of theory (except for CCSD(T) and all-electron calculations) relative to H + Th^+. Values include spin−orbit correction of the difference between the ^2D state averaged over all spin−orbit states and the $^4F_{3/2}$ ground level (−0.40 eV). [b]Single point energy using B3LYP optimized structures. [c]ThH^+ ($^3\Delta_1$). Includes spin−orbit stabilization energy of the $^3\Delta_1$ level (0.18 eV). [d]ThH^+ ($^1\Sigma^+$). [e]Complete basis set limit extrapolated from correlation consistent basis sets using the extrapolation technique described in the text. [f]Single point energy from B3LYP/cc-pwCVQZ-MDF/aug-cc-pVQZ optimized structure.

electrons of thorium ζ_{6d}(Th). We have previously estimated ζ_{6d}(Th) as 1458 cm^{-1} (0.18 eV).[30]

Spin−Orbit Energy Corrections for ThH^+. Previously di Santo et al. have reported a $^3\Delta$ ground state with a $^1\Sigma^+$ state 0.02 eV higher in energy in B3LYP/SDD-VDZ-MWB/6-311+G(p) calculations.[21] We also reported similar results using B3LYP/Seg. SDD-VQZ-MWB/6-311+G(3p) where we observed a $^3\Delta$ ground state with excited states at 0.18 ($^3\Pi$) and 0.30 eV ($^1\Sigma^+$).[30] CCSD(T)/Seg. SDD-VQZ-MWB/6-311+G(3p) results reverse the order placing the $^1\Sigma^+$ 0.07 eV below the $^3\Delta$, and CCSD(T)/cc-pVQZ-MDF/cc-pVTZ calculations place the $^1\Sigma^+$ only 0.04 eV below the $^3\Delta$.[30] These results do not include corrections for spin−orbit energy. When spin−orbit effects were included, the ground level was $^3\Delta_1$ at all levels of theory studied.[30]

The present work finds similar results to the previous reports. In order to compare theoretical results more readily to experimental values, spin−orbit effects are estimated using eq 9. These results are summarized in Table 3. The $^1\Sigma^+$ and $^3\Sigma^-$ states have no first order spin−orbit corrections, whereas the $^3\Delta$ splits into Ω = 1, 2, 3; $^3\Pi$ splits into Ω = 0, 1, 2; and $^3\Phi$ splits into Ω = 2, 3, 4. For $^3\Delta$, where Λ = 2 and M_S = −1, 0, and +1, eq 9 shows that A = 729 cm^{-1} and E^{SO} = −0.18, 0, and 0.18 eV for $^3\Delta_1$, $^3\Delta_2$, $^3\Delta_3$, respectively. For $^3\Pi$ (Λ = 1 and M_S = −1, 0, 1), E^{SO} = −0.09, 0, and 0.09 eV for $^3\Pi_0$, $^3\Pi_1$, and $^3\Pi_2$, respectively. For $^3\Phi$ (Λ = 3 and M_S = −1, 0, 1), E^{SO} = −0.27, 0, 0.27 eV for $^3\Phi_2$, $^3\Phi_3$, $^3\Phi_4$, respectively. Once these spin−orbit corrections have been applied, the ground level is predicted to be $^3\Delta_1$ (by 0.13−0.69 eV) for all levels of theory except M06 which predicts that the $^1\Sigma^+$ is 0.10 eV lower in energy. This trend is also reflected in the calculations using additional basis sets, Table S3 in the Supporting Information.

The $^3\Delta$ state has a $1\sigma^2 2\sigma 1\delta$ electron configuration. A natural bond orbital analysis (NBO) performed using CCSD(T) indicates that the 1σ bonding orbital comprises the H 1s-orbital and a sd-hybridized orbital that also contains some f-character (70% 6d, 20% 7s, 10% 5f). The nonbonding 2σ-orbital comprises mostly the Th^+ 7s-orbital (75%) with some 6d-character (20%). The nonbonding 1δ-orbital is composed entirely of the Th^+ 6dδ-orbital. The $^1\Sigma^+$ state has a $1\sigma^2 2\sigma^2$ electron configuration. These orbitals are similar to those for the $^3\Delta$ with an NBO analysis using CCSD(T) indicating that the 1σ bonding interaction occurs between the H 1s and an orbital on Th^+ having 75% 6d, 15% 7s, and 10% 5f character, whereas the nonbonding 2σ-orbital has 85% 7s and 15% 6d. For the higher energy states, the $^3\Pi$ state has a $1\sigma^2 2\sigma 1\pi$ electron configuration where the 1δ-electron in the $^3\Delta$ state is moved to a π-orbital that is the Th^+ 6dπ-orbital, and the $^3\Phi$ has a $1\sigma^2 1\delta 1\pi$ electron configuration. For the two $^3\Sigma^-$ states, the two nonbonding electrons are placed in either the Th^+ 6dδ or 6dπ-orbitals.

The $^3\Delta$ and $^3\Pi$ states can originate from the Th^+ (^4F, $6d^27s$) + H (^2S) and possibly the ^2D ($6d7s^2$) + H (^2S) asymptotes, whereas the $^1\Sigma^+$ can originate only from the Th^+ (^2D, $6d7s^2$) + H (^2S) asymptote, and the $^3\Phi$ and $^3\Sigma^-$ states likely come from the Th^+ (^4F, $6d^3$) + H (^2S) asymptote. Here, Th^+ is an interesting case because the assigned ground level is $^4F_{3/2}$; however, the J = $^3/_2$ ground level is actually a mixture of the $^4F_{3/2}$ and $^2D_{3/2}$ levels indicating that all states of ThH^+ presumably can be formed directly from the Th^+ ground level. The $^3\Sigma^-$ states can also form from the ground level or from the Th^+ (^4F, $6d^3$) state. In this regard, it can be noted that the excitation energies of the $^3\Sigma^-$ states are similar to the difference (0.83 eV) between the ground $^4F_{3/2}$ ($6d^27s$) and $^4F_{3/2}$ ($6d^3$) levels of Th^+.

Bond lengths, r(Th^+−H), and vibrational frequencies (scaled by 0.989)[82] calculated for the various states of ThH^+ using B3LYP/cc-pwCVQZ-MDF/aug-cc-pVQZ are listed in Table 3. To the best of our knowledge, neither experimental nor theoretical molecular parameters have been reported previously for ThH^+. Bond lengths vary from r(Th^+−H) = 1.946 ($^1\Sigma^+$) to 2.032 ($^3\Phi$) Å with r(Th^+−H) = 1.996 Å for the $^3\Delta$. Vibrational frequencies range from 1491 ($^3\Phi$) to 1653 ($^3\Delta$) with ν = 1592 cm^{-1} for $^1\Sigma^+$. Parameters calculated at other levels of theory are listed in Tables S4 and S5 in the Supporting Information.

Table 4 lists the theoretical BDEs of ground level ThH^+ at various levels of theory and basis set combinations. The ground state is $^3\Delta_1$ after accounting for spin−orbit energy for all levels of theory except M06, which finds a $^1\Sigma^+$ ground state. However, because of the close proximity in energy of the $^1\Sigma^+$ and $^3\Delta_1$

DOI: 10.1021/acs.jpcb.5b08008
J. Phys. Chem. B 2016, 120, 1601−1614

Table 5. Calculated Molecular Parameters and Relative Energies (eV) for Ground and Excited States of $HThH^+$[a]

state	configuration	$r(Th^+-H)$ (Å)[b]	∠HThH (deg)[b]	CCSD(T)	B3LYP	B3PW91	BHLYP	M06	PBE0
$^2A_1$	$(1a_1)^2(1b_2)^2(2a_1)^1$	1.995	102.3	0.00	0.00	0.00	0.00	0.00	0.00
				(−1.47)	(−1.62)	(−1.70)	(−1.51)	(−1.59)	(−1.72)
$^2B_1$	$(1a_1)^2(1b_2)^2(1b_1)^1$	2.021	103.5	0.35	0.29	0.25	0.29	0.11	0.26
$^2A_2$	$(1a_1)^2(1b_2)^2(1a_2)^1$	2.017	90.7	0.48	0.40	0.38	0.44	0.18	0.39
$^2B_2$	$(1a_1)^2(1b_2)^2(2b_2)^1$	2.051	95.1	1.30	0.78	0.75	1.02	0.43	0.80
$^4A_2$	$(1a_1)^2(1b_2)^1(2a_1)^1(1b_1)^1$	2.160	169.1	2.93	2.77	2.75	2.89	3.13	2.76
		2.302	*20.0*	*1.22*	*1.36*	*1.23*	*1.38*	*1.49*	*1.22*
$^4B_2$	$(1a_1)^2(1b_2)^1(2a_1)^1(3a_1)^1$	2.160	169.1	2.93	2.77	2.76	2.89	3.12	2.76
		2.334	*19.8*	*1.25*	*1.34*	*1.20*	*1.34*	*1.52*	*1.19*
$^4B_1$	$(1a_1)^2(1b_2)^1(1a_2)^1(2a_1)^1$	2.108	169.9	2.98	3.05	2.99	3.22	3.16	2.79
		2.327	*19.9*	*1.33*	*1.33*	*1.19*	*1.34*	*1.51*	*1.18*
$^4A'$[c]		2.160	180.0	2.93	2.77	2.76	2.89	3.12	2.76
$^4A_1$	$(1a_1)^2(1b_2)^1(2a_1)^1(2b_2)^1$	*2.349*	*19.8*	*2.30*	*1.79*	*1.71*	*2.03*	*1.78*	*1.74*
$^4A_2$	$(1a_1)^2(1b_2)^1(1a_2)^1(2b_2)^1$	2.093	170.1	3.52	3.69	3.48	3.83	3.54	3.46
		2.318	*20.5*	*2.95*	*2.45*	*2.26*	*2.63*	*2.34*	*2.29*

[a]Single point energies of B3LYP/cc-pwCVQZ-MDF/aug-cc-pVQZ optimized structures. Values in parentheses are relative to Th^+ (^2D) + H_2. Values in italics distinguish minima found at small ∠HThH angles along the indicated diabatic potential energy surface. [b]From B3LYP/cc-pwCVQZ-MDF/aug-cc-pVQZ optimized structures. [c]$^4A_1$ state collapses to $^4A'$ at large angles. See text.

states, a definitive determination of the true ground state is difficult. Consequently, the calculated BDEs of both states can be found in Table S6 in the Supporting Information. (Table S6 also contains values uncorrected for spin−orbit splitting and for additional basis sets.) In general, the ground state BDEs overestimate the experimental bond strength by 0.2−0.5 eV with CCSD(T) (2.71 eV), BHLYP (2.75 eV), and M06 (2.73 eV) values being in closest agreement to experiment when using the cc-pwCVQZ-MDF/aug-cc-pVQZ basis sets. Notably, spin−orbit corrections yield better results in all cases, Table S6.

The DFT cc-pwCVQZ-MDF/aug-cc-pVQZ results listed in Table 4 are typical of the DFT results regardless of the basis set combination; however, CCSD(T) calculations vary appreciably. Among the basis sets that utilize an ECP, the smallest basis set, CCSD(T)/SDD-VDZ-MWB/6-311+G(3p), reproduces $D_0(Th^+-H)$ within experimental uncertainty, and the larger CCSD(T)/Seg. SDD-VQZ-MWB/6-311+G(3p) and CCSD(T)/ANO-VQZ-MWB/6-311+G(3p) results are just outside of experimental uncertainty. Meanwhile the use of a similarly sized CCSD(T)/ANO-VQZ-MDF/6-311+G(3p) basis set with the fully relativistic basis set (MDF) leads to results that overestimate the bond strength considerably for both states. This substantial deviation is not understood but suggests that this basis set may not be well-optimized for Th^+. An extrapolation to the complete basis set limit using the cc-pwCVXZ-MDF (X= T, Q) basis sets leads to CCSD(T)/CBS-cc-pwCVXZ-MDF results similar to CCSD(T)/cc-pwCVQZ-MDF/aug-cc-pVQZ results. The BDEs of the CBS limit for the all-electron basis sets (CBS-cc-pwCVXZ-DK3) are 0−0.11 eV lower than their counterparts that utilize the MDF ECP (CBS-cc-pwCVXZ-DK3).

Fully Relativistic Calculations on ThH^+. To investigate the role of second order spin−orbit effects on the ordering of the $^3\Delta_1$ and $^1\Sigma^+$, fully relativistic Dirac Hartree−Fock calculations are performed where the spin-orbitals are generated using the average-of-configuration SCF approach, and all states are projected out with a full CI in this spin-orbital space. These calculations are performed with the DIRAC14 code[95] using an uncontracted Dyall basis set for thorium[96] and an uncontracted Dunning basis set for hydrogen.[67] The standard finite nucleus model of the DIRAC14 code is used, and all two-electron integrals including the Gaunt interaction[97] responsible for the spin-other-orbit interaction are included in the calculations. Two different orbital configuration spaces are utilized, with one large space representing the Th 5f, 6d, 7s, and H 1s and a second small space with 8 spin-orbitals that describe 17 spin−orbit split states including the lowest levels for $^3\Delta$, $^1\Sigma^+$, $^3\Pi$, and $^3\Phi$. The calculated $^3\Delta$ spin−orbit splitting constants of 0.17 and 0.16 eV for the large and small space, respectively, are slightly smaller than the 0.18 eV estimated from the atomic thorium 6d splitting. Relative energies for the $^3\Delta_1$, $^3\Delta_2$, and $^3\Delta_3$ states obtained from these calculations are −0.14, 0.00, and 0.20 eV for the large configuration space and −0.13, 0.00, and 0.19 eV for the small space, respectively. Here the $^3\Delta_2$ is defined as zero to allow for a direct comparison with the results obtained from eq 9. The relative energies show that the second order effects are relatively small, on the order of 0.02−0.03 eV. In both configuration spaces used, the $^3\Delta_1$ state is the ground state with the $^1\Sigma^+$ state 0.03 and 0.10 eV higher in energy for the large and small space, respectively. The relative energy differences between the $^3\Delta_1$ and $^1\Sigma^+$ states obtained in the fully relativistic calculations are similar, although somewhat smaller, as compared to the CCSD(T) calculations combined with eq 9, suggesting the model is a reasonable approach to estimate the effect of spin−orbit splitting in these systems.

Potential Energy Surface for $HThH^+$. Calculated ground and excited states of $HThH^+$ are listed in Table 5. The ground state, $^2A_1$, has bond distances, $r(Th^+-H)$, of 1.995 Å, and a bond angle, ∠HThH, of 102.3° (B3LYP/cc-pwcVQZ-MDF/aug-cc-pVQZ). The $^2B_1$, $^2A_2$, and $^2B_2$ states lie 0.11−0.35, 0.18−0.48, and 0.43−1.30 eV higher in energy, respectively. A series of quartet states were also located at both small and large ∠HThH bond angles and lie at least 1.18 eV above the $^2A_1$ ground state. Linear variants of $HThH^+$ were also calculated but were all found to have one negative vibrational frequency indicating that these are transition states. Similar results were observed for linear $ThHH^+$ variants. Theory predicts that the $^2A_1$ state has a BDE, $D_0(Th^+-H_2)$, relative to $Th^+(^4F_{3/2})$ + H_2 of 1.07−1.32 eV with $D_0(HTh^+-H)$ = 2.73−2.96 eV. Note that the second hydride bond energy is comparable to the first,

DOI: 10.1021/acs.jpcb.5b08008
J. Phys. Chem. B 2016, 120, 1601−1614

consistent with covalent coupling of H to one of the unpaired electrons in ThH^+ ($^3\Delta$).

The $^2A_1$ state has a $(1a_1)^2(1b_2)^2(2a_1)^1$ electron configuration where the lone electron is found in an orbital ($2a_1$) composed primarily of the Th^+ (7s). The $1a_1$ bonding orbital is an sd hybridized orbital interacting with the H (1s) orbitals, and the $1b_2$ orbital is a bonding interaction of the $6d_{yz}$ (where the z-axis is defined as the C_2 symmetry axis and the molecule lies in the yz-plane) and the H (1s) orbitals. For the $^2B_1$ state, the lone electron is moved into the $6d_{xz}$ orbital, and for the $^2A_2$ state, the electron is moved into the $6d_{xy}$ orbital. The $^2B_2$ state places the lone electron in the antibonding $2b_2$ orbital, leading to its higher energy.

For the quartet states, one of the bonding electrons must be moved to a nonbonding or antibonding orbital, such that these states lie considerably higher in energy. In the large angle variants, all with ∠HThH near 170°, this also leads to slightly longer Th^+–H bond lengths, ~2.1 Å. For each of these states, minima are also observed at small ∠HThH angles, Table 5, corresponding to $Th^+(H_2)$ association complexes. In general, the geometries of these intermediates are characterized by ∠HThH of ~20° with r(H–H) of approximately 0.8 Å, similar to r(H–H) = 0.739–0.744 Å calculated for free H_2. Additionally, $r(Th^+\text{-}H)$ = 2.30–2.35 Å are observed, which are significantly longer than the bond lengths of the large angle $HThH^+$ species (2.0–2.1 Å).

In order to further explore the potential energy surface of reaction 5, we performed relaxed potential energy scans along the ∠HThH coordinate using the optimized $HThH^+$ structures as a starting geometry. In our theoretical study of the Th^+ + CH_4 reaction,[30] the DFT methods yielded similar results regardless of the basis set used. Consequently, to avoid excessive computational cost, scans were performed using the B3LYP/Seg. SDD-VQZ-MWB/6-311+G(3p) level of theory. The results of these scans are presented in Figure 5. Notably, neither zero point energies nor spin–orbit effects are included in this diagram. Additionally, for the cc-pwCVQZ-MDF/aug-cc-pVQZ calculations, a $^4A_1$ intermediate is found at small angles; however, at larger angles the $^4A_1$ intermediate has 1 imaginary frequency along the asymmetric Th^+–H stretch suggesting that it is the inversion transition state to a $^4A'$ intermediate. Indeed, optimization of a geometry displaced along the imaginary frequency using the $^4A_1$ wave function leads to a $^4A'$ state with $r(Th^+\text{–}H)$ = 2.1599 and 2.1601 Å. An analysis of the orbitals indicates that the symmetry of the orbitals is similar to the $^4A_1$ $[(1a_1)^2(1b_2)^1(2a_1)^1(2b_2)^1]$ found using the Seg. SDD-VQZ-MWB/6-311+G(3p) basis set. The break from C_{2v} symmetry using the larger basis sets is possibly caused by the degeneracy of the $^4A_1$ and $^4B_2$ states at linearity. Neither the $^4A_1$ nor $^4B_2$ surfaces are expected to play a prominent role in reaction 5.

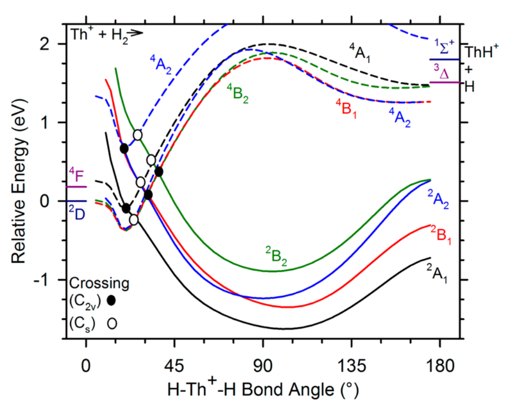

Figure 5. B3LYP/Seg. SDD-VQZ-MWB/6-311+(3p) relaxed potential energy surface scan calculations of the Th^+ + H_2 reaction in C_{2v} symmetry as a function of $\angle HTh^+H$ in degrees. The energies are relative to Th^+ (^2D, $6d7s^2$) + H_2. Doublet surfaces are represented by solid lines and quartet surfaces by dashed lines. Surface crossings that would be avoided in C_{2v} and C_s symmetry (ignoring spin) are indicated by the solid and open circles.

Initially, all doublet surfaces are repulsive, so approach of Th^+ with H_2 in reaction 3 evolves along a quartet surface where the $^4A_2$, $^4B_1$, and $^4B_2$ surfaces are similar in energy (see also Table 5). Qualitatively, this can be understood on the basis of the doubly occupied 7s frontier orbital of Th^+ (^2D), versus its single occupation in the ^4F state. Note that the quartet surfaces for the $HThH^+$ species evolve at small angles to energies that match that calculated for Th^+ (^2D) + H_2. This disparity appears to be a result of the spin-contamination of the calculated ^2D asymptote, as none of the surfaces shown in Figure 5 exhibit any appreciable spin-contamination. At larger angles, these quartet surfaces cross that of the $^2A_1$ surface that leads to the global minimum. On this surface, two covalent bonds with the H-ligands are formed via interactions of the Th^+ 6d-electrons with the H 1s-electrons so that the unpaired electron is found in the $2a_1$(7s) orbital. Loss of a H ligand from these doublet spin intermediates can potentially lead to high spin-coupled ThH^+ ($^3\Delta$, $^3\Pi$, $^3\Phi$) + H (^2S) or low spin-coupled ThH^+ ($^1\Sigma^+$) + H (^2S) products with no barrier in excess of the asymptotic energies. Overall, these surfaces show that the reaction of Th^+ ($J = {}^3/_2$) with H_2 can occur via the formation of a stable dihydride intermediate with no barrier in the entrance or exit channels presuming that the quartet and doublet surfaces couple, which seems likely given the large spin–orbit interactions in this heavy metal system. This coupling with the low-spin surface would lead to category 1 (statistical) behavior that is consistent with the mechanism indicated by the branching ratio of reactions 7 and 8, Figure 4.

■ DISCUSSION

Basis Set Comparison. Table 4 shows that BDEs derived from DFT methods vary little between basis sets used for Th^+ and H; however, CCSD(T) results may differ by as much as 0.3 eV (excluding CCSD(T)/ANO-VQZ-MDF/6-311+G(3p)) between basis sets. For CCSD(T), basis sets that utilize quasirelativistic MWB (SDD-VDZ-MWB, ANO-VQZ-MWB, and Seg. SDD-VQZ-MWB) are in better agreement with the experimental BDE than those calculated using the fully relativistic MDF ECP (ANO-VQZ-MDF and cc-pwCVXZ-MDF). For DFT, BDEs calculated using the all-electron cc-pwCVXZ-DK3 and cc-pVXZ-DK3 basis sets are 0–0.13 eV smaller than their ECP counterparts (except B3LYP/cc-pwCVQZ-DK3 which is 0.01 eV larger), cc-pwCVXZ-MDF and cc-pVXZ-MDF, respectively (see also Table S6). For CCSD(T) calculations, the all-electron and ECP cc-pwCVXZ-MDF basis sets yield identical results, whereas the cc-pVXZ-DK3 basis sets yield BDEs 0.0–0.03 eV smaller than their ECP counterpart.

Interestingly, the smaller basis sets appear to reproduce the experimental BDE best. This is not likely a cause of the basis set superposition error (BSSE) as calculations indicate that the BSSE is only 0.03 eV (not included in Table 4) for the largest basis set combination CCSD(T)/cc-pwCVQZ-MDF/aug-cc-

DOI: 10.1021/acs.jpcb.5b08008
J. Phys. Chem. B 2016, 120, 1601–1614

pVQZ. This is also shown by the small difference in the cc-pwCVQZ-MDF and CBS values. Similarly, errors resulting from the use of the MDF ECP appear to be minimal as the difference between CBS-cc-pwCVXZ-MDF and CBS-cc-pwCVXZ-DK3 results are small, Table 4.

In a previous study, CCSD(T)/cc-pVQZ-MDF/cc-pVTZ calculations overpredicted the BDE of singly bound ThH^+ ($^3\Delta_1$) and $ThCH_3^+$ ($^1A_1$) by 0.22 and 0.62 eV, respectively, but performed much better than the smaller basis sets for the triply bound $ThCH^+$ ($^1\Sigma^+$), underpredicting the experimental value by 0.21 eV.[30] Similarly, CBS limit extrapolations using correlation consistent basis sets are also lower than the experimental value by 0.2 eV for several transition metal oxide cation BDEs.[91,92] For calculations involving several other ThL^+ species, it was found that high levels of theory, CCSDT(Q) and multireference configuration interaction (MRCI+Q) calculations, were necessary to reproduce experimental relative energies of the ground and excited states. Specific errors relative to the experimental difference between the ground and first excited state (0.08 eV) were 0.06 eV for CCSD(T), 0.03 eV for CCSDT(Q), and 0.01_5 eV for MRCI+Q.[31,77] This was attributed to accurate recovery of correlation energy.[31] The use of these very high levels of theory are not attempted here and could be the cause for the discrepancies between the experimental and calculated BDEs.

The spin contamination in the Th^+ (^2D) ion indicates significant mixing of spin states, which points to the need for multireference quantum calculations to obtain the relative energies of the states at high accuracy. Although the mixed character is presumably accounted for in the empirical correction factor, the multireference character of the Th^+ (^2D) asymptote could potentially be mitigated by calculating the BDE in reference to a "pure" state and correcting by the empirical excitation energy to the ground state. For the CCSD(T)/cc-pwCVQZ-MDF/aug-cc-pVQZ calculations referenced to the excited Th^+ (^2F) + H (^2S) configuration (excitation energy from $J = {}^3/_2$ ground level = 0.83 eV), the BDE is 2.86 eV, in worse agreement with the experimental value than the approach used here.

ThH^+ Electronic State. Previous theoretical work on ThH^+ by di Santo et al.[21] identified a $^3\Delta$ ground state with a low-lying (0.02 eV) $^1\Sigma^+$ excited state (B3LYP/SDD-VDZ-MWB/6-311+G(p)). In the present work, all levels of theory except CCSD(T) and M06 identify the $^3\Delta$ as the ground state before accounting for spin−orbit interaction. After including spin−orbit corrections, all levels of theory except M06 indicate that the ground level is $^3\Delta_1$. Nevertheless, the close proximity of the $^3\Delta$ and $^1\Sigma^+$ states makes unambiguous determination of the ground state difficult; therefore, a comparison to similar species may be useful in providing additional insight into identification of the ThH^+ ground state.

One such comparison is to HfH^+, which like ThH^+ has either a $^1\Sigma^+$ or $^3\Delta$ ground state,[44,98,99] where the $^1\Sigma^+$ ($1\sigma^2 2\sigma^2$) can only be formed from the Hf^+ (^2D, $5d6s^2$) + H (^2S, 1s) asymptote and the $^3\Delta$ ($1\sigma^2 2\sigma 1\delta$) state is formed from the Hf^+ (^4F, $5d^26s$) + H asymptote (possibly the Hf^+ (^2D, $5d6s^2$) + H (^2S, 1s) asymptote). Because the 2σ molecular orbital (MO) is essentially the Hf^+ 6s-orbital, the 1σ bonding orbital in the $^1\Sigma^+$ cannot be sd-hybridized resulting in poor orbital overlap and a weaker BDE than the $^3\Delta$ where sd-hybridization of the Hf^+ bonding orbital is allowed.[44] Because the Hf^+ ground state is ^2D (with a $^2D_{3/2}$ ground level),[89] the ground state of HfH^+ is $^1\Sigma^+$ if the stabilization resulting from an sd−s MO over a d−s MO is less than the promotion energy, E_p = 0.45 eV,[89] from the ground level $^2D_{3/2}$ to the $^4F_{3/2}$ level. Unlike Hf^+, Th^+ has a $J = {}^3/_2$ ground level with 43% $^4F_{3/2}$ and 27% $^2D_{3/2}$ mixed character,[88] so that both the $^1\Sigma^+$ and $^3\Delta$ states can presumably evolve directly from the ground level asymptote. Assuming that there is an advantage to forming the ThH^+ bond using a sd-hybridized orbital, then the likely ground state of ThH^+ is $^3\Delta$. This simplistic analysis ignores likely second order interactions between low-lying states of ThH^+, which the fully relativistic calculations discussed above indicate are small.

Recently there has been an effort to characterize actinide chemical bonds spectroscopically. Although ThH has been studied in an Ar matrix,[100] ThH^+ has not been studied. ThF^+, which has been studied in pulsed-field ionization zero kinetic energy (PFI-ZEKE) photoelectron spectroscopy and laser-induced fluorescence (LIF) experiments,[31,77] may be expected to have similar characteristics as ThH^+ because both ligands have one unpaired electron and form a single covalent bond with Th^+. PFI-ZEKE experiments indicate that either the $^3\Delta_1$ or $^1\Sigma^+$ is the ground level of ThF^+.[31,77] Later LIF results confirmed a $^1\Sigma^+$ ground level, with the $^3\Delta_1$ level only 316 cm^{-1} (0.04 eV) higher in energy.[31] These results are consistent with high-level quantum chemical calculations that include spin−orbit coupling, which place both the $^3\Delta$ or $^1\Sigma^+$ states as low-lying, similar to ThH^+. Bonding occurs by an interaction of the F $2p_z$-orbital with an appropriate Th^+ orbital (most likely an sd-hybridized orbital). The 1δ-orbital in the $^3\Delta$ state was found to be a Th^+ $6d\delta$-orbital, and the filled 2σ-orbital in the $^1\Sigma^+$ state is primarily the Th^+ 7s-orbital.[31] Heaven et al.[31] also note a slight antibonding interaction between the Th^+ $6d\pi$-orbitals and the F $2p\pi$-orbitals, an effect that cannot occur for ThH^+ because the H ligand has no occupied p-orbitals.

Qualitatively, the difference in the character of the π-orbitals in ThH^+ and ThF^+ suggests that the $^3\Pi$ state of ThH^+ should be lower in energy than the analogous ThF^+ $^3\Pi$ state. This is confirmed by experimental and theoretical results. Experimentally, the $^3\Pi_0$ level is found 0.42 eV above the $^1\Sigma^+$ ground state in ThF^+ (the $^3\Pi_1$ was not observed in the range 0−4000 cm^{-1}),[77] whereas theoretical calculations indicate that the $^3\Pi_0$ and $^3\Pi_1$ lie 0.61 and 0.65 eV above the ground state, respectively.[31] In ThH^+, theoretical calculations (CCSD(T)/cc-pwCVQZ-MDF/aug-cc-pVQZ) combined with empirical spin−orbit effects estimated using eq 9 indicate that the $^3\Pi_0$ and $^3\Pi_1$ lie 0.39 and 0.48 eV above the $^3\Delta_1$ ground level (0.28 and 0.37 eV above the $^1\Sigma^+$), respectively.

The energy of the $^3\Pi$ levels has implications for the second order interaction of the $^1\Sigma^+$ and $^3\Delta_1$ levels with the $^3\Pi_0$ and $^3\Pi_1$ levels, respectively. Because theoretical calculations in the present work indicate that the $^1\Sigma^+$ and $^3\Pi_0$ levels are closer in energy in ThH^+ than ThF^+, it is anticipated that the second order interaction between these levels will be stronger than the interaction between the same levels in ThF^+. Likewise, the interaction of the $^3\Delta_1$ and $^3\Pi_1$ levels in ThH^+ will also be stronger than the corresponding levels in ThF^+. For ThF^+, theoretical calculations that explicitly treat spin−orbit interaction place the $^3\Pi_0$ and $^3\Pi_1$ levels only 0.04 eV apart compared to a 0.09 eV difference expected using eq 9, suggesting that the second order interaction of the $\Omega = 0$ levels stabilizes the $^1\Sigma^+$ state by 0.05 eV. Interestingly, the difference in energy of the $^1\Sigma^+$ (ground) and $^3\Delta_1$ states is only 0.02 eV calculated at the same level of theory (0.04 eV experimentally).[31] Thus, the second order interaction with the $^3\Pi_0$ level is influential in making the $^1\Sigma^+$ state of ThF^+ the ground level.

DOI: 10.1021/acs.jpcb.5b08008
J. Phys. Chem. B 2016, 120, 1601−1614

Given that the $^3\Pi$ state is likely closer in energy to the $^1\Sigma^+$ and $^3\Delta$ states in ThH^+ than in ThF^+, estimated spin−orbit effects from eq 9 suggest that the states are probably very close in energy. Overall, the ThH^+ ground state is most likely $^3\Delta_1$, but it is difficult to make a definitive assignment absent experimental data. Notably, given the reported difficulty in assigning the analogous ThF^+ ground state spectroscopically,[31] the ThH^+ ground state will likely also be difficult to assign experimentally. As noted above, explicit fully relativistic calculations accounting for multireference character and spin−orbit interactions continue to confirm this close spacing, with the $^3\Delta_1$ state being the ground state and the $^1\Sigma^+$ state 0.03−0.10 eV higher in energy, comparable to the 0.13 eV spacing found using the empirical spin−orbit correction.

MH^+ Thermochemistry. Because Th^+, unlike other actinides, does not populate the 5f-orbitals in its ground state, a good comparison can be made to transition metals with three valence electrons, Ti^+, Zr^+, and Hf^+. These have BDEs of $D_0(Ti^+{-}H) = 2.31 \pm 0.11$,[38] $D_0(Zr^+{-}H) = 2.26 \pm 0.08$,[41] and $D_0(Hf^+{-}H) = 2.11 \pm 0.08$ eV,[44] as measured in guided ion beam experiments analogous to the present ones. The lower Hf^+ BDE has been explained as resulting from the fully occupied 6s orbital in the ^2D ($5d6s^2$) ground state of Hf^+.[44] The other transition metal congeners have ^4F (d^2s) ground states that permit ready formation of a strong $M^+(s){-}H(s)$ or $M^+(sd){-}H(s)$ covalent bond. The ground level of Th^+ is a mixture of ^4F and ^2D states, which does not appear to inhibit the bond strength as $D_0(Th^+{-}H)$ is 0.2−0.3 eV stronger than $D_0(Ti^+{-}H)$ and $D_0(Zr^+{-}H)$. This trend is similar to that reported for BDEs of the same metals with other ligands and can be attributed to the lanthanide contraction, where increasing nuclear charge preferentially contracts the s-orbital allowing for efficient sd-hybridization and better M^+−ligand orbital overlap.[30,43,101−105]

According to theory, the participation of the d-orbitals in group 4 MH^+ bonding increases moving down the periodic table. Previous theoretical work has indicated that sd-hybridization is typically not important for first-row transition metals. Consequently, TiH^+ has a $^3\Phi$ ground state[106] that can form directly from the Ti^+ ^4F ($3d^24s$) ground state via $M^+(s){-}H(s)$ bonding. sd-hybridization becomes more important in ZrH^+ as suggested by the close proximity of the $^3\Delta$ and $^3\Phi$ states. Both states have been reported as the ground state in different studies,[41,106] and both states can be formed directly from the Zr^+ ^4F ($4d^25s$) ground state through $M^+(sd){-}H(s)$ or $M^+(s){-}H(s)$ bonding, respectively. For the third-row transition metals, sd-hybridization becomes important because of the similarity in size of the 4s and 5d orbitals.[98] For HfH^+, the ground state is most likely $^3\Delta$, which can be formed from the low-lying ^4F ($5d^26s$) state.[44] Likewise, the present work indicates that the bonding interaction between Th^+ and H occurs between an orbital primarily 6dσ in character and the H 1s orbital for the likely ground state, $^3\Delta$ (presumably because the 7s orbital is now too large to overlap well with the 1s orbital of H, unlike the smaller transition metal congeners).

The BDE trend can be explained with promotion energy (E_p) arguments where E_p is defined as the difference in energy between the M^+ ground level and the first level with an appropriate electronic configuration (d^2s) for bonding. This definition ignores any spin decoupling effects[107] but should be qualitatively correct. Both Ti^+ and Zr^+ have $^4F_{3/2}$ (d^2s) ground levels, so $E_p = 0.0$ eV. Hf^+ has a $^2D_{3/2}$ ($5d6s^2$) ground level, and the first level with the appropriate configuration is $^4F_{3/2}$ ($5d^26s$), $E_p = 0.45$ eV. Likewise, ThH^+ most likely has a $^3\Delta$ ground state, and the Th^+ $J = {}^3/_2$ ground level has primarily an appropriate configuration ($6d^27s$). This yields intrinsic BDEs ($= D_0 + E_p$) of 2.31 ± 0.11, 2.26 ± 0.08, 2.56 ± 0.08, and 2.45 ± 0.07 eV for TiH^+, ZrH^+, HfH^+, and ThH^+, respectively, which increase roughly as the metal gets heavier (within experimental uncertainty), as might be anticipated for the trend associated with the lanthanide contraction. It is also possible that the ThH^+ BDE is depressed by the $^2D_{3/2}$ ($6d7s^2$) character mixed into the $J = {}^3/_2$ ground level, such that the promotion energy is better described as corresponding to a more pure ^4F level, e.g., the $^4F_{5/2}$ (65% ^4F, 17% ^2D), 0.19 eV above the ground level,[88] leading to an intrinsic BDE of 2.64 eV. Nevertheless, because the effect of the ^2D character on the ThH^+ BDE is not clear, we adopt $E_p(Th^+) = 0.0$ eV.

AnH^+ Thermochemistry. In this section, we explore whether the thermochemistry of Th^+ determined here can be analyzed to provide insight into the thermochemistry of other actinide (An) systems where the thermochemistry is poorly understood. In a recent study of the reactions of An^{2+} with alkanes and alkenes using ICR, several AnH^+ species were observed in reactions at thermal temperatures.[18] For the purposes of determining lower limits to the AnH^+ BDE, the most discriminating process is reaction 10.

$$An^{2+} + C_3H_8 \rightarrow AnH^+ + C_3H_7^+ \tag{10}$$

Reaction 10 was observed at thermal energies yielding UH^+, NpH^+, PuH^+, AmH^+, and CmH^+ with product branching percentages of 10, 5, 70, 90, and 10%, respectively.[18] Thus, the ICR results suggest that a lower limit to the AnH^+ BDE can be obtained using eq 11:

$$D_0(An^+{-}H) \geq D_0(H_7C_3{-}H) - IE(An^+) + IE(C_3H_7) \tag{11}$$

Here $D_0(H_7C_3{-}H) = 4.20 \pm 0.02$ eV[83,108,109] and $IE(C_3H_7) = 7.37 \pm 0.02$ eV.[83,110] Only $IE(U^+) = 10.6$ eV[111] and $IE(Pu^+) = 11.2$ eV[112] are listed in a review of atomic energy levels,[89] values that yield lower limits of $D_0(U^+{-}H) \geq 0.97 \pm 0.2$ eV and $D_0(Pu^+{-}H) \geq 0.37 \pm 0.2$ eV, where we have assumed an uncertainty of ±0.2 eV for $IE(An^+)$. In contrast, in an evaluation of $IE(An^+)$ by Marçalo and Gibson,[9] $IE(U^+) = 11.7 \pm 0.3$ eV and $IE(Pu^+) = 11.8 \pm 0.3$ eV are given, values that indicate reaction 10 is exothermic no matter how weak the AnH^+ bond may be.

Other than our recent work on ThH^+,[30] the only previous experimental report of an AnH^+ BDE is that of $D_0(U^+{-}D) = 2.9 \pm 0.1$ eV measured in early (notably *not* guided) ion beam studies of the reactions of U^+ with CD_4 and D_2.[10] In later theoretical work, di Santo et al. report UH^+ BDEs calculated using B3LYP/SDD-VDZ-MWB/6-311+G(p) and PW91/ZORA as 2.35 and 2.94 eV, respectively.[21] Although the PW91/ZORA value is in good agreement with the experimental value in this case, this level of theory appears to overestimate bond strength in other molecules where experimental data is readily available.[21,30] The difference in energy of the ThH^+ and UH^+ BDEs is potentially interesting because the measured UH^+ BDE is ~0.5 eV stronger than the ThH^+ BDE, which is opposite the results from theoretical BDEs reported by di Santo et al. that predict ThH^+ to be the stronger bond at both levels of theory investigated.[21]

As discussed above, AnF^+ species are potentially similar to the AnH^+ systems. BDEs of $D_0(Th^+{-}F) = 6.63 \pm 0.10$ eV,[31,89,113] $D_0(U^+{-}F) = 6.57 \pm 0.10$ eV,[31,89,114] and

DOI: 10.1021/acs.jpcb.5b08008
J. Phys. Chem. B 2016, 120, 1601−1614

Table 6. Estimation of AnL^+ Bond Dissociation Energies (eV) from An^+ Electronic Parameters[a]

		$D_0(An^+-F)$		$D_0(An^+-CH_3)$		$D_0(An^+-H)$	
An^+ ground config[b]	promotion energy[b]	exptl	estimate	exptl	estimate	exptl	estimate
Ac^+ ($7s^2$)	0.59 (6d7s)		6.04		2.01		1.86
Th^+ ($6d^27s$)	0.00 ($6d^27s$)	6.63 ± 0.10[c]	6.63	2.60 ± 0.30[d]	2.60	2.45 ± 0.07	2.45
Pa^+ ($5f^27s^2$)	0.10 ($5f^26d7s$)		6.53	≥0.29 ± 0.30[e]	2.50		2.35
U^+ ($5f^37s^2$)	0.04 ($5f^36d7s$)	6.57 ± 0.10[f]	6.59	≥1.29 ± 0.10[e]	2.56	2.9 ± 0.1[g]	2.41
Np^+ ($5f^46d7s$)	0.00 ($5f^46d7s$)		6.63	≥0.34 ± 0.30[e]	2.60		2.45
Pu^+ ($5f^67s$)	1.08 ($5f^56d7s$)	5.40 ± 0.34[h]	5.55	≥0.69 ± 0.10[e]	1.52	≥ 0.37 ± 0.10[e]	1.37
Am^+ ($5f^77s$)	1.76 ($5f^76d$)		4.87		0.84		0.69
Cm^+ ($5f^77s^2$)	0.50 ($5f^76d7s$)		6.13		2.10		1.95

[a]Estimate of AnL^+ BDEs using ThL^+ BDEs as an estimate of the intrinsic AnL^+ BDE, i.e., $D_0(An^+-L) = D_0(Th^+-L) - E_P(An^+)$. See text. [b]Promotion energy defined as the difference in energy between the ground level and the lowest-lying level with the indicated electronic configuration. Energy levels and configurations from refs 88 and 89. [c]Calculated from D_0(Th−F) = 6.72 ± 0.10 eV,[113] IE(Th) = 6.3067 eV,[89] and IE(ThF) = 6.3953 ± 0.0004 eV.[31] [d]Reference 30. [e]Lower limits derived from results of ICR reaction $An^{2+} + C_3H_8$ from ref 18 using eq 10 (or analogous equation). Hydrocarbon BDEs and IEs from ref 83. IEs for U^+ and Pu^+ from ref 89. Other IE(An^{2+}) from ref 9. [f]Calculated from D_0(U−F) = 6.72 ± 0.10 eV,[114] IE(U) = 6.1941 eV,[89] and IE(UF) = 6.341 59 ± 0.000 06 eV.[31] [g]Reference 10. [h]Calculated from D_0(Pu−F) = 5.58 ± 0.30 eV[115] and IE(Pu) = 6.026 eV.[89] Ionization energy of PuF estimated as IE(PuF) = 6.2 eV. See discussion in the Supporting Information.

$D_0(Pu^+-F)$ = 5.40 ± 0.34 eV[89,115] can be derived from existing reports using the thermochemical cycle (see the Supporting Information for a full discussion). Assuming that the AnH^+ BDE trend is similar to that of the AnF^+ trend, this analysis indicates that the ThH^+ and UH^+ BDEs should be similar, which clearly suggests that the reported UH^+ BDE is too large. Of note is the much larger AnF^+ BDEs compared to AnH^+, a result consistent with bonds that are significantly more ionic than the AnH^+ bonds along with contributions from donation of F(2pπ) electrons into empty An^+ (6dπ) orbitals. Nevertheless, the required electronic configuration of An^+ (discussed below) to form a single covalent bond to either the H or F ligand is the same in both AnH^+ and AnF^+ so that the periodic trends comparison should be qualitatively correct.

The trends in these three BDEs can also be understood in terms of the promotion energy from the ground level to a reactive level with the appropriate configuration, $E_P(An^+)$.[9] For AnL^+ with a bond order of 1, the required electron configuration could be $5f^{n-1}7s$, $5f^{n-2}6d7s$, $5f^{n-2}6d^2$, or $5f^{n-3}6d^27s$. As noted above with Th^+, the 7s-orbital appears to be insufficient to form a strong covalent bonding interaction, such that promotion to a configuration with at least one 6d electron is needed. Notably, the difference in BDEs between UF^+ and ThF^+ is similar to the magnitude of $E_P(U^+)$ = 0.04 eV[89] from the ground level $^4I_{9/2}$ ($5f^37s^2$) to $^6L_{11/2}$ ($5f^36d7s$) for U^+. Likewise, the difference between the ThF^+ and PuF^+ BDEs is comparable to E_p = 1.08 eV[89] from the ground level $^8F_{1/2}$ ($5f^67s$) to $^8K_{7/2}$ ($5f^56d7s$) for Pu^+ (a result that confirms that a 6d electron is needed for bonding). Previously, Marçalo and Gibson have shown that the BDEs for AnO^{n+} (n = 0−2) are correlated to the promotion energy of An^{n+} to the first state with a $6d^2$ electron configuration because two valence electrons on the metal are needed to form a strong bond with O.[9] Because the typical configuration of early An^+ is $5f^{n-2}7s^2$,[89] this correlation indicates that non-f electrons are required for strong bonding. The intrinsic BDE (diabatic BDE arising from the An reactive state), $D_0(An^{n+}-L)^*$, for that configuration should also be similar across the AnO^{n+} series. For n = 1, a reasonable estimate for this intrinsic BDE is $D_0(Th^+-L)$ because Th^+ has a ground configuration of $6d^27s$. This allows for the simple model shown in eq 12

$$D_0(An^+-L)^* = D_0(Th^+-L) = D_0(An^+-L) + E_P(An^+) \quad (12)$$

where $E_P(An^+)$ is the promotion energy from the ground level to a reactive level with the appropriate configuration (again ignoring the energy associated with spin decoupling the bonding electron from other unpaired electrons on the metal).[9] Equation 12 allows for the estimate of $D_0(An^+-L)$ from established $D_0(Th^+-L)$. Consequently, we estimate the BDEs of AnF^+, AnH^+, and $AnCH_3^+$ for Ac−Cm in Table 6, where $D_0(Th^+-CH_3)$ was determined previously from the reaction $Th^+ + CH_4$.[30]

■ CONCLUSIONS

Analysis of the kinetic energy dependence of the cross sections in Figures 1−3 indicates that $D_0(Th^+-H)$ = 2.45 ± 0.07 eV. This value is in agreement with the previously reported $D_0(Th^+-H)$ ≥ 2.25 ± 0.20 eV measured in the reaction $Th^+ + CH_4$ as well as the PST model of the same system, which indicates a BDE of 2.45 eV.[30] Branching ratios from reactions 7 and 8 indicate that the reaction proceeds via a statistical mechanism. This is thought to occur from coupling of the mixed character surfaces of the Th^+ ground level to several doublet surfaces, which lead to long-lived ThH_2^+ intermediates. In general, theoretical BDEs overestimate the bond strength of ThH^+ even after including spin−orbit contributions, which always improve the agreement. Furthermore, the use of the larger cc-pwCVQZ-MDF and cc-pVQZ-MDF basis sets (that include *i*-functions) does not improve theoretical results compared to the smaller SDD-VDZ and Seg. SDD-VQZ. This may indicate that higher levels of theory than CCSD(T) may be necessary to accurately describe these actinide BDEs. However, CCSD(T) and BHLYP results are in reasonable agreement with the experimental value obtained here and also reproduce atomic state orderings reasonably well. Previous calculations for the various products of the $Th^+ + CH_4$ system indicate that CCSD(T) calculations provide the best agreement with experimental BDEs, while BHLYP performs well only for singly bound systems.[30]

■ ASSOCIATED CONTENT

Supporting Information

The Supporting Information is available free of charge on the ACS Publications website at DOI: 10.1021/acs.jpcb.5b08008.

Relative energies and molecular parameters for ThH^+ ground and excited states calculated at additional levels

DOI: 10.1021/acs.jpcb.5b08008
J. Phys. Chem. B 2016, 120, 1601−1614

of theory and ThH^+ BDEs calculated at additional levels of theory (PDF)

AUTHOR INFORMATION

Corresponding Author

*E-mail: armentrout@chem.utah.edu. Phone: +1 (801) 581-7885.

Notes

The authors declare no competing financial interest.

ACKNOWLEDGMENTS

This work is supported by the Heavy Element Chemistry Program, Office of Basic Energy Sciences, U.S. Department of Energy, Grant No. DE-SC0012249. We thank the Center for High Performance Computing at the University of Utah for the generous allocation of computer time. This research used resources of the Oak Ridge Leadership Computing Facility, which is a DOE Office of Science User Facility supported under Contract DE-AC05-00OR22725. An award of computer time was provided by the Innovative and Novel Computational Impact on Theory and Experiment (INCITE) program.

REFERENCES

(1) Armentrout, P. B.; Beauchamp, J. L. Reactions of U^+ and UO^+ with O_2, CO, CO_2, COS, CS_2, and D_2O. *Chem. Phys.* **1980**, *50*, 27−36.

(2) Armentrout, P. B.; Beauchamp, J. L. Collision-Induced Dissociation of UO^+ and UO_2^+. *Chem. Phys.* **1980**, *50*, 21−25.

(3) Cornehl, H. H.; Wesendrup, R.; Diefenbach, M.; Schwarz, H. A Comparative Study of Oxo-Ligand Effects in the Gas-Phase Chemistry of Atomic Lanthanide and Actinide Cations. *Chem. - Eur. J.* **1997**, *3*, 1083−1090.

(4) Gibson, J. K.; Haire, R. G. Gas-Phase Chemistry of Bare and Oxo-Ligated Protactinium Ions: A Contribution to a Systematic Understanding of Actinide Chemistry. *Inorg. Chem.* **2002**, *41*, 5897−5906.

(5) Santos, M.; Marcalo, J.; Pires de Matos, A.; Gibson, J. K.; Haire, R. G. Gas-Phase Oxidation Reactions of Neptunium and Plutonium Ions Investigated via Fourier Transform Ion Cyclotron Resonance Mass Spectrometry. *J. Phys. Chem. A* **2002**, *106*, 7190−7194.

(6) Gibson, J. K. Role of Atomic Electronics in f-Element Bond Formation: Bond Energies of Lanthanide and Actinide Oxide Molecules. *J. Phys. Chem. A* **2003**, *107*, 7891−7899.

(7) Gibson, J. K.; Haire, R. G.; Santos, M.; Marcalo, J.; Pires de Matos, A. Oxidation Studies of Dipositive Actinide Ions, An^{2+} (An = Th, U, Np, Pu, Am) in the Gas Phase: Synthesis and Characterization of the Isolated Uranyl, Neptunyl, and Plutonyl Ions UO_2^{2+}(g), NpO_2^{2+}(g), and PuO_2^{2+}(g). *J. Phys. Chem. A* **2005**, *109*, 2768−2781.

(8) Gibson, J. K.; Haire, R. G.; Marcalo, J.; Santos, M.; Leal, J. P.; Pires de Matos, A.; Tyagi, R.; Mrozik, M. K.; Pitzer, R. M.; Bursten, B. E. FTICR/MS Studies of Gas-Phase Actinide Ion Reactions: Fundamental Chemical and Physical Properties of Atomic and Molecular Actinide Ions and Neutrals. *Eur. Phys. J. D* **2007**, *45*, 133−138.

(9) Marcalo, J.; Gibson, J. K. Gas-Phase Energetics of Actinide Oxides: An Assessment of Neutral and Cationic Monoxides and Dioxides from Thorium to Curium. *J. Phys. Chem. A* **2009**, *113*, 12599−12606.

(10) Armentrout, P. B.; Hodges, R. V.; Beauchamp, J. L. Endothermic Reactions of Uranium Ions with N_2, D_2 and CD_4. *J. Chem. Phys.* **1977**, *66*, 4683−4688.

(11) Marcalo, J.; Leal, J. P.; Pires de Matos, A. Gas Phase Actinide Ion Chemistry: Activation of Alkanes and Alkenes by Thorium Cations. *Int. J. Mass Spectron. Ion Processes* **1996**, *157-158*, 265−274.

(12) Gibson, J. K. Gas-Phase Transuranium Organometallic Chemistry: Reactions of Np^+, Pu^+, NpO^+, and PuO^+ with Alkenes. *J. Am. Chem. Soc.* **1998**, *120*, 2633−2640.

(13) Gibson, J. K. Actinide Gas-Phase Chemistry: Reactions of An^+ and AnO^+ [An = Th, U, Np, Pu, Am] with Nitriles and Butylamine. *Inorg. Chem.* **1999**, *38*, 165−173.

(14) Gibson, J. K. Gas-Phase Reactions of An^+ and AnO^{n+} [An = Th, U, Np, Pu, Am] with halogenated hydrocarbons [$C_{14}F_{24}$, C_3F_6, $C_2H_4Cl_2$, and $C_2H_4Br_2$]. *Radiochim. Acta* **1999**, *84*, 135−146.

(15) Gibson, J. K.; Haire, R. G. Berkelium and Californium Organometallic Ions. *Radiochim. Acta* **2001**, *89*, 363−369.

(16) Gibson, J. K.; Haire, R. G.; Marçalo, J.; Santos, M.; Pires de Matos, A.; Mrozik, M. K.; Pitzer, R. M.; Bursten, B. E. Gas-Phase Reactions of Hydrocarbons with An^+ and AnO^+ (An = Th, Pa, U, Np, Pu, Am, Cm): The Active Role of 5f Electrons in Organoprotactinium Chemistry. *Organometallics* **2007**, *26*, 3947−3956.

(17) di Santo, E.; Santos, M.; Michelini, M. C.; Marcalo, J.; Russo, N.; Gibson, J. K. Gas-Phase Reactions of the Bare Th^{2+} and U^{2+} Ions with Small Alkanes, CH_4, C_2H_6, and C_3H_8: Experimental and Theoretical Study of Elementary Organoactinide Chemistry. *J. Am. Chem. Soc.* **2011**, *133*, 1955−1970.

(18) Marcalo, J.; Santos, M.; Gibson, J. K. Gas-Phase Reactions of Doubly Charged Actinide Cations with Alkanes and Alkenes-Probing the Chemical Activity of 5f Electrons from Th to Cm. *Phys. Chem. Chem. Phys.* **2011**, *13*, 18322−18329.

(19) de Almeida, K. J.; Cesar, A. Methane C-H Bond Activation by Neutral Lanthanide and Thorium Atoms in the Gas Phase: A Theoretical Prediction. *Organometallics* **2006**, *25*, 3407−3416.

(20) Mazzone, G.; Michelini, M. d. C.; Russo, N.; Sicilia, E. Mechanistic Aspects of the Reaction of Th^+ and Th^{2+} with Water in the Gas Phase. *Inorg. Chem.* **2008**, *47*, 2083−2088.

(21) di Santo, E.; Michelini, M. d. C.; Russo, N. Methane C−H Bond Activation by Gas-Phase Th^+ and U^+: Reaction Mechanisms and Bonding Analysis. *Organometallics* **2009**, *28*, 3716−3726.

(22) di Santo, E.; Michelini, M. C.; Russo, N. Activation of Ethane C-H and C-C Bonds by Gas Phase Th^+ and U^+: A Theoretical Study. *J. Phys. Chem. A* **2009**, *113*, 14699−14705.

(23) de Almeida, K. J.; Duarte, H. A. Gas-Phase Methane Activation by the Ac+−Pu+ Ions: Theoretical Insights into the Role of 5f Electrons/Orbitals in Early Actinide Chemistry. *Organometallics* **2009**, *28*, 3203−3211.

(24) de Almeida, K. J.; Duarte, H. A. Dehydrogenation of Methane by Gas-Phase Th, Th^+, and Th^{2+}: Theoretical Insights into Actinide Chemistry. *Organometallics* **2010**, *29*, 3735−3745.

(25) Zhou, J.; Schlegel, H. B. Ab Initio Molecular Dynamics Study of the Reaction between Th^+ and H_2O. *J. Phys. Chem. A* **2010**, *114*, 8613−8617.

(26) Infante, I.; Kovacs, A.; Macchia, G. L.; Shahi, A. R. M.; Gibson, J. K.; Gagliardi, L. Ionization Energies for the Actinide Mono- and Dioxides Series, from Th to Cm: Theory versus Experiment. *J. Phys. Chem. A* **2010**, *114*, 6007−6015.

(27) Kovacs, A.; Konings, R. J. M. Computed Vibrational Frequencies of Actinide Oxides $AnO^{0/+/2}+$ and $AnO_2^{0/+/2+}$ (An = Th, Pa, U, Np, Pu, Am, Cm). *J. Phys. Chem. A* **2011**, *115*, 6646−6656.

(28) Averkiev, B. B.; Mantina, M.; Valero, R.; Infante, I.; Kovacs, A.; Truhlar, D. G.; Gagliardi, L. How Accurate are Electronic Structure Methods for Actinoid Chemistry? *Theor. Chem. Acc.* **2011**, *129*, 657−666.

(29) Pereira, C. C. L.; Marsden, C. J.; Marcalo, J.; Gibson, J. K. Actinide Sulfides in the Gas Phase: Experimental and Theoretical Studies of the Thermochemistry of AnS (An = Ac, Th, Pa, U, Np, Pu, Am and Cm). *Phys. Chem. Chem. Phys.* **2011**, *13*, 12940−12958.

(30) Cox, R. M.; Armentrout, P. B.; de Jong, W. A. Activation of CH_4 by Th^+ as Studied by Guided Ion Beam Mass Spectrometry and Quantum Chemistry. *Inorg. Chem.* **2015**, *54*, 3584−3599.

(31) Heaven, M. C.; Barker, B. J.; Antonov, I. O. Spectroscopy and Structure of the Simplest Actinide Bonds. *J. Phys. Chem. A* **2014**, *118*, 10867−10881.

(32) Elkind, J. L.; Armentrout, P. B. Effect of kinetic and electronic energy on the reaction of V+ with H_2, HD, and D_2. *J. Phys. Chem.* **1985**, *89*, 5626−5636.

(33) Elkind, J. L.; Armentrout, P. B. Effect of Kinetic and Electronic Energy on the Reactionss of Fe^+ with H_2, HD and D_2: State-Specific Cross Sections for $Fe^+(^6D)$ and $Fe^+(^4F)$. *J. Phys. Chem.* **1986**, *90*, 5736−5745.
(34) Elkind, J. L.; Armentrout, P. B. Effect of Kinetic and Electronic Energy on the Reactions of Mn^+ with H_2, HD and D_2. *J. Chem. Phys.* **1986**, *84*, 4862−4871.
(35) Elkind, J. L.; Armentrout, P. B. Effect of Kinetic and Electronic Energy on the Reactions of Co^+, Ni^+ and Cu^+ with H_2, HD and D_2. *J. Phys. Chem.* **1986**, *90*, 6576−6586.
(36) Elkind, J. L.; Armentrout, P. B. Transition Metal Hydride Bond Energies: First and Second Row. *Inorg. Chem.* **1986**, *25*, 1078−1080.
(37) Elkind, J. L.; Armentrout, P. B. Effect of Kinetic and Electronic Energy on the reactions of Cr^+ with H_2, HD, and D_2. *J. Chem. Phys.* **1987**, *86*, 1868−1877.
(38) Elkind, J. L.; Armentrout, P. B. Effect of Kinetic and Electronic Energy on the Reactions of Ti^+ with H_2, HD and D_2. *Int. J. Mass Spectrom. Ion Processes* **1988**, *83*, 259−284.
(39) Elkind, J. L.; Sunderlin, L. S.; Armentrout, P. B. Periodic Trends in Chemical Reactivity: Reactions of Sc^+, Y^+, La^+, and Lu^+ with H_2, D_2, and HD. *J. Phys. Chem.* **1989**, *93*, 3151−3158.
(40) Chen, Y.-M.; Elkind, J. L.; Armentrout, P. B. Reactions of Ru^+, Rh^+, Pd^+, and Ag^+ with H_2, HD, and D_2. *J. Phys. Chem.* **1995**, *99*, 10438−10445.
(41) Sievers, M. R.; Chen, Y.-M.; Elkind, J. L.; Armentrout, P. B. Reactions of Y^+, Zr^+, Nb^+, and Mo^+ with H_2, HD, and D_2. *J. Phys. Chem.* **1996**, *100*, 54−62.
(42) Zhang, X.-G.; Armentrout, P. B. Reactions of Pt^+ with H_2, D_2, and HD: Effect of Lanthanide Contraction on Reactivity and Thermochemistry. *J. Chem. Phys.* **2002**, *116*, 5565−5573.
(43) Zhang, X.-G.; Rue, C.; Shin, S.-Y.; Armentrout, P. B. Reactions of Ta^+ and W^+ with H_2, D_2, and HD: Effect of Lanthanide Contraction and Spin-Orbit Interactions on Reactivity and Thermochemistry. *J. Chem. Phys.* **2002**, *116*, 5574−5583.
(44) Hinton, C. S.; Armentrout, P. B. Guided Ion Beam and Theoretical Study of the Reactions of Hf^+ with H_2, D_2, and HD. *J. Chem. Phys.* **2010**, *133*, 124307.
(45) Hinton, C. S.; Citir, M.; Armentrout, P. B. Guided Ion Beam and Theoretical Study of the Reactions of Os^+ with H_2, D_2, and HD. *J. Chem. Phys.* **2011**, *135*, 234302.
(46) Li, F.; Hinton, C. S.; Citir, M.; Liu, F.; Armentrout, P. B. Guided Ion Beam and Theoretical Study of the Reactions of Au^+ with H_2, D_2, and HD. *J. Chem. Phys.* **2011**, *134*, 024310.
(47) Sugiyama, K.; Yoda, J. Production of YbH^+ by Chemical Reaction of Yb^+ in Excited States with H_2 Gas. *Phys. Rev. A: At., Mol., Opt. Phys.* **1997**, *55*, R10−R13.
(48) Sunderlin, L. S.; Armentrout, P. B. Periodic Trends in Chemical Reactivity. Reactions of Sc^+, Y^+, La^+, and Lu^+ with Methane and Ethane. *J. Am. Chem. Soc.* **1989**, *111*, 3845−3855.
(49) Marcalo, J.; Santos, M.; Pires de Matos, A.; Gibson, J. K.; Haire, R. G. Gas-Phase Reactions of Doubly Charged Lanthanide Cations with Alkanes and Alkenes. Trends in Metal(2+) Reactivity. *J. Phys. Chem. A* **2008**, *112*, 12647−12656.
(50) Loh, S. K.; Hales, D. A.; Lian, L.; Armentrout, P. B. Collision-Induced Dissociation of Fe_n^+ (n = 2 - 10) with Xenon: Ionic and Neutral Iron Binding Energies. *J. Chem. Phys.* **1989**, *90*, 5466−5485.
(51) Schultz, R. H.; Armentrout, P. B. Reactions of N_4^+ with Rare Gases from Thermal to 10 eV Center-of-Mass Energy: Collision-Induced Dissociation, Charge Transfer and Ligand Exchange. *Int. J. Mass Spectrom. Ion Processes* **1991**, *107*, 29−48.
(52) Teloy, E.; Gerlich, D. Integral Cross Sections for Ion−Molecule Reactions. I. The Guided Beam Technique. *Chem. Phys.* **1974**, *4*, 417−427.
(53) Gerlich, D. Inhomogeneous RF fields: A VersatileTool for the Study of Processes with Slow Ions. *Adv. Chem. Phys.* **1992**, *82*, 1−176.
(54) Daly, N. R. Scintillation-Type Mass Spectrometer Ion Detector. *Rev. Sci. Instrum.* **1960**, *31*, 264−267.
(55) Ervin, K. M.; Armentrout, P. B. Translational Energy Dependence of $Ar^+ + XY \rightarrow ArX^+ + Y$ ($XY = H_2,D_2,HD$) from Thermal to 30 eV c.m. *J. Chem. Phys.* **1985**, *83*, 166−189.
(56) Chantry, P. J. Doppler Broadening in Beam Experiments. *J. Chem. Phys.* **1971**, *55*, 2746−2759.
(57) Haynes, C. L.; Armentrout, P. B. Thermochemistry and Structures of $CoC_3H_6^+$: Metallacycle and Metal-Alkene Isomers. *Organometallics* **1994**, *13*, 3480−3490.
(58) Kickel, B. L.; Armentrout, P. B. Reactions of Fe+, Co+, and Ni+ with Silane. Electronic State Effects, Comparison to Reactions with Methane, and M+-SiHx (x = 0−3) Bond Energies. *J. Am. Chem. Soc.* **1995**, *117*, 764−773.
(59) Kickel, B. L.; Armentrout, P. B. Guided Ion Beam Studies of the Reactions of Group 3 Metal Ions (Sc^+, Y^+, La^+, and Lu^+) with Silane. Electronic State Effects, Comparison to Reactions with Methane, and M^+-SiH_x (x = 0−3) Bond Energies. *J. Am. Chem. Soc.* **1995**, *117*, 4057−4070.
(60) Clemmer, D. E.; Chen, Y.-M.; Khan, F. A.; Armentrout, P. B. State-Specific Reactions of $Fe^+(a^6D, a^4F)$ with D_2O and Reactions of FeO^+ with D_2. *J. Phys. Chem.* **1994**, *98*, 6522−6529.
(61) Armentrout, P. B. Kinetic Energy Dependence of Ion−Molecule Reactions: Guided Ion Beams and Threshold Measurements. *Int. J. Mass Spectrom.* **2000**, *200*, 219−241.
(62) Chesnavich, W. J.; Bowers, M. T. Theory of Translationally Driven Reactions. *J. Phys. Chem.* **1979**, *83*, 900−905.
(63) Muntean, F.; Armentrout, P. B. Guided Ion Beam Study of Collision-Induced Dissociation Dynamics: Integral and Differential Cross Sections. *J. Chem. Phys.* **2001**, *115*, 1213−1228.
(64) Frisch, M. J.; Trucks, G. W.; Schlegel, H. B.; Scuseria, G. E.; Robb, M. A.; Cheeseman, J. R.; Scalmani, G.; Barone, V.; Mennucci, B.; Petersson, G. A.; et al. *Gaussian 09, Revision A.1*; Gaussian, Inc: Wallingford, CT, 2009.
(65) Peterson, K. A. Correlation Consistent Basis Sets for Actinides. I. The Th and U atoms. *J. Chem. Phys.* **2015**, *142*, 074105.
(66) Weigand, A.; Cao, X.; Hangele, T.; Dolg, M. Relativistic Small-Core Pseudopotentials for Actinium, Thorium, and Protactinium. *J. Phys. Chem. A* **2014**, *118*, 2519−2530.
(67) Dunning, T. H., Jr. Gaussian Basis sets for Use in Correlated Molecular Calculations. I. The Atoms Boron Through Neon and Hydrogen. *J. Chem. Phys.* **1989**, *90*, 1007−1023.
(68) Feller, D. The Role of Databases in Support of Computational Chemistry Calculations. *J. Comput. Chem.* **1996**, *17*, 1571−1586.
(69) Schuchardt, K. L.; Didier, B. T.; Elsethagen, T.; Sun, L.; Gurumoorthi, V.; Chase, J.; Li, J.; Windus, T. L. Basis Set Exchange: A Community Database for Computational Sciences. *J. Chem. Inf. Model.* **2007**, *47*, 1045−1052.
(70) Cao, X.; Dolg, M.; Stoll, H. Valence Basis Sets for Relativistic Energy-Consistent Small-Core Actinide Pseudopotentials. *J. Chem. Phys.* **2003**, *118*, 487−496.
(71) Douglas, M.; Kroll, N. M. Quantum Electrodynamical Corrections to the Fine Structure of Helium. *Ann. Phys. (Amsterdam, Neth.)* **1974**, *82*, 89−155.
(72) Hess, B. A. Applicability of the No-Pair Equation with Free-Particle Projection Operators to Atomic and Molecular Structure Calculations. *Phys. Rev. A: At., Mol., Opt. Phys.* **1985**, *32*, 756−763.
(73) Hess, B. A. Relativistic Electronic-Structure Calculations Employing a Two-Component No-Pair Formalism with External-Field Projection Operators. *Phys. Rev. A: At., Mol., Opt. Phys.* **1986**, *33*, 3742−3748.
(74) Jansen, G.; Hess, B. A. Revision of the Douglas-Kroll Transformation. *Phys. Rev. A: At., Mol., Opt. Phys.* **1989**, *39*, 6016−6017.
(75) de Jong, W. A.; Harrison, R. J.; Dixon, D. A. Parallel Douglas-Kroll Energy and Gradients in NWChem: Estimating Scalar Relativistic Effects using Douglas-Kroll Contracted Basis Sets. *J. Chem. Phys.* **2001**, *114*, 48−53.
(76) Barysz, M.; Sadlej, A. J. Two-Component Methods of Relativistic Quantum Chemistry: from the Douglas-Kroll Approx-

DOI: 10.1021/acs.jpcb.5b08008
J. Phys. Chem. B 2016, 120, 1601−1614

imation to the Exact Two-Component Formalism. *J. Mol. Struct.: THEOCHEM* **2001**, *573*, 181−200.
(77) Barker, B. J.; Antonov, I. O.; Heaven, M. C.; Peterson, K. A. Spectroscopic Investigations of ThF and ThF^+. *J. Chem. Phys.* **2012**, *136*, 104305.
(78) Karton, A.; Martin, J. M. L. Comment on: ″Estimating the Hartree-Fock Limit from Finite Basis Set Calculations″ [Jensen F (2005) Theor Chem Acc 113:267]. *Theor. Chem. Acc.* **2006**, *115*, 330−333.
(79) Martin, J. M. L. Ab Initio Total Atomization Energies of Small Molecules - Towards the Basis Set Limit. *Chem. Phys. Lett.* **1996**, *259*, 669−678.
(80) Feller, D.; Peterson, K. A.; Hill, J. G. On the Effectiveness of CCSD(T) Complete Basis Set Extrapolations for Atomization Energies. *J. Chem. Phys.* **2011**, *135*, 044102.
(81) Holthausen, M. C.; Heinemann, C.; Cornehl, H. H.; Koch, W.; Schwarz, H. The Performance of Density-Functional/Hartree-Fock Hybrid Methods: Cationic Transition-Metal Methyl Complexes MCH_3^+ (M = Sc-Cu,La,Hf-Au). *J. Chem. Phys.* **1995**, *102*, 4931−4941.
(82) Foresman, J. B.; Frisch, A. E. *Exploring Chemistry with Electronic Structure Methods*, 2nd ed.; Gaussian, Inc.: Pittsburgh, PA, 1996.
(83) Johnson, R. D., III. *NIST Computational Chemistry Comparison and Benchmark Database NIST Standard Reference Database Number 101 Release 16a*; August 2013.
(84) Weber, M. E.; Elkind, J. L.; Armentrout, P. B. Kinetic Energy Dependence of $Al^+ + O_2 \rightarrow AlO^+$ + atomic O. *J. Chem. Phys.* **1986**, *84*, 1521−1529.
(85) Armentrout, P. B. Periodic Trends in the Reactions of Atomic Ions with Molecular Hydrogen. *Int. Rev. Phys. Chem.* **1990**, *9*, 115−148.
(86) Burley, J. D.; Ervin, K. M.; Armentrout, P. B. Translational Energy Dependence of $O^+(^4S)$ + $H_2(D_2$, HD) − > $OH^+(OD^+)$ + H(D) from Thermal to 30 eV c.m. *Int. J. Mass Spectrom. Ion Processes* **1987**, *80*, 153−175.
(87) Armentrout, P. B. Isotope Effects in the Reactions of Atomic Ions with H_2, D_2, and HD. *ACS Symp. Series* **1992**, *502*, 194−209.
(88) Blaise, J.; Wyart, J.-F. *International Tables of Selected Constants, Energy Levels, and Atomic Spectra of Actinides*; Tables of Constants and Numerical Data; Paris, 1992; Vol. *20*. http://web2.lac.u-psud.fr/lac/Database/Contents.html (accessed 2/9/2015).
(89) Sansonetti, J. E.; Martin, W. C. Handbook of Basic Atomic Spectroscopic Data. *J. Phys. Chem. Ref. Data* **2005**, *34*, 1559−2259.
(90) Garcia, M. A.; Morse, M. D. Resonant Two-Photon Ionization Spectroscopy of Jet-Cooled OsN: 520−418 nm. *J. Chem. Phys.* **2011**, *135*, 114304.
(91) Armentrout, P. B. The Bond Energy of ReO^+: Guided Ion-Beam and Theoretical Studies of the Reaction of Re^+ (^7S) with O_2. *J. Chem. Phys.* **2013**, *139*, 084305.
(92) Armentrout, P. B.; Li, F.-X. Bond Energy of IrO^+: Guided Ion-Beam and Theoretical Studies of the Reaction of Ir+ (^5F) with O_2. *J. Phys. Chem. A* **2013**, *117*, 7754−7766.
(93) Armentrout, P. B.; Parke, L.; Hinton, C.; Citir, M. Activation of Methane by Os+: Guided-Ion-Beam and Theoretical Studies. *ChemPlusChem* **2013**, *78*, 1157−1173.
(94) Lefebvre-Brion, H.; Field, R. W. *The Spectra And Dynamics of Diatomic Molecules*; Elsevier: Amsterdam, 2004.
(95) Saue, T.; Visscher, L.; Jensen, H.; Bast, R.; Bakken, V.; Dyall, K. G.; Dubillard, S.; Ekström, U.; Eliav, E.; Enevoldsen, T.; et al. *DIRAC, a Relativistic ab Initio Electronic Structure Program, Release DIRAC14*; 2014; see http://www.diracprogram.org.
(96) Dyall, K. G. Relativistic Double-Zeta, Triple-Zeta, and Quadruple-Zeta Basis Aets for the Actinides Ac-Lr. *Theor. Chem. Acc.* **2007**, *117*, 491−500.
(97) Gaunt, J. A. The Triplets of Helium. *Proc. R. Soc. London, Ser. A* **1929**, *122*, 513−532.
(98) Ohanessian, G.; Brusich, M. J.; Goddard, W., III A.Theoretical Study of Transition-metal Hydrides. 5. HfH^+ through HgH^+, BaH^+, and LaH^+. *J. Am. Chem. Soc.* **1990**, *112*, 7179−7189.
(99) Meyer, E. R.; Bohn, J. L.; Deskevich, M. P.Candidate Molecular Ions for an Electron Electric Dipole Moment Experiment. *Phys. Rev. A: At., Mol., Opt. Phys.* **2006**, *73*, 062108.
(100) Souter, P. F.; Kushto, G. P.; Andrews, L.; Neurock, M. Experimental and Theoretical Evidence for the Isolation of Thorium Hydride Molecules in Argon Matrixes. *J. Phys. Chem. A* **1997**, *101*, 1287−1291.
(101) Zhang, X.-G.; Liyanage, R.; Armentrout, P. B. The Potential Energy Surface for Activation of Methane by Pt^+: A Detailed Guided-Ion Beam Study. *J. Am. Chem. Soc.* **2001**, *123*, 5563−5575.
(102) Armentrout, M. M.; Li, F.-X.; Armentrout, P. B. Is Spin Conserved in Heavy Metal Systems? Experimental and Theoretical Studies of the Reaction of Re+ with Methane. *J. Phys. Chem. A* **2004**, *108*, 9660−9672.
(103) Armentrout, P. B. Activation of CH_4 by Gas-Phase Mo^+ and the Thermochemistry of Mo-Ligand Complexes. *J. Phys. Chem. A* **2006**, *110*, 8327−8338.
(104) Li, F.-X.; Zhang, X.-G.; Armentrout, P. B. The Most Reactive Third-row Transition Metal: Guided Ion Beam and Theoretical Studies of the Activation of Methane by Ir^+. *Int. J. Mass Spectrom.* **2006**, *255-256*, 279−300.
(105) Zhang, X.; Schwarz, H. Bonding in Cationic MCH_2^+ (M = K−La, Hf−Rn): A Theoretical Study on Periodic Trends. *Chem. - Eur. J.* **2010**, *16*, 5882−5888.
(106) Pettersson, L. G. M.; Bauschlicher, C. W., Jr.; Langhoff, S. R.; Partridge, H. Positive Ions of the First- and Second-row Transition Metal Hydrides. *J. Chem. Phys.* **1987**, *87*, 481−492.
(107) Carter, E. A.; Goddard, W. A. IIIRelationships Between Bond Energies in Coordinatively Unsaturated and Coordinatively Saturated Transition-Metal Complexes: a Quantitative Guide for Single, Double, and Triple bonds. *J. Phys. Chem.* **1988**, *92*, 5679−5683.
(108) Berkowitz, J.; Ellison, G. B.; Gutman, D. Three Methods to Measure RH Bond Energies. *J. Phys. Chem.* **1994**, *98*, 2744−2765.
(109) Frenkel, M. M. K. N.; Wilhoit, R. C.; Kabo, G. J.; Roganov, G. N. *Thermodynamics of Organic Compounds in the Gas State*; Thermodynamics Research Center: College Station, TX, 1994.
(110) Dyke, J.; Ellis, A.; Jonathan, N.; Morris, A. Vacuum Ultraviolet Photoelectron Spectroscopy of Transient Species. Part 18. The Cyclopropyl, Isopropyl, and n-Propyl Radicals. *J. Chem. Soc., Faraday Trans. 2* **1985**, *81*, 1573−1586.
(111) Steinhaus, D. W.; Radziemski, L. J., Jr.; Cowan, R. D. *Current Status of the Analysis of the Optical Spectra of Uranium*; University of California: Oakland, CA, 1971; pp 151−63.
(112) Worden, E. F.; Carlson, L. R.; Johnson, S. A.; Paisner, J. A.; Solarz, R. W. Ionization Potential of Neutral Atomic Plutonium Determined by Laser Spectroscopy. *J. Opt. Soc. Am. B* **1993**, *10*, 1998−2005.
(113) Lau, K. H.; Brittain, R. D.; Hildenbrand, D. L. High Temperature Thermodynamic Studies of Some Gaseous Thorium Fluorides. *J. Chem. Phys.* **1989**, *90*, 1158−1164.
(114) Hildenbrand, D. L.; Lau, K. H. Redetermination of the Thermochemistry of Gaseous Uranium Fluorides (UF_5, UF_2, and UF). *J. Chem. Phys.* **1991**, *94*, 1420−1425.
(115) Kent, R. A. Mass Spectrometric Studies of Plutonium Compounds at High Temperatures. II. Enthalpy of Sublimation of Plutonium(III) Fluoride and the Dissociation Energy of Plutonium(I) Fluoride. *J. Am. Chem. Soc.* **1968**, *90*, 5657−5659.

DOI: 10.1021/acs.jpcb.5b08008
J. Phys. Chem. B 2016, 120, 1601−1614